# Arrhythmias precede cardiomyopathy and remodeling of Ca2+ handling proteins in a novel model of long QT syndrome

Jérôme Montnach, Franck Chizelle, Nadjet Belbachir, Claire Castro, Linwei Li, Gildas Loussouarn, Gilles Toumaniantz, Agnès Carcouët, Anne Julia Meinzinger, Doron Shmerling, et al.

# Arrhythmias precede cardiomyopathy and remodeling of $Ca^{2+}$ handling proteins in a novel model of long QT syndrome

Jérôme Montnach,[1*#] Franck F. Chizelle,[1#] Nadjet Belbachir,[1] Claire Castro,[1] Linwei Li,[3] Gildas Loussouarn,[1] Gilles Toumaniantz,[1] Agnès Carcouët,[1] Anne Julia Meinzinger,[4] Doron Shmerling,[4] Jean-Pierre Benitah,[3] Ana Maria Gómez,[3] Flavien Charpentier[1,2§], Isabelle Baró[1§]

[1] l'institut du thorax, INSERM, CNRS, UNIV Nantes, Nantes, France

[2] l'institut du thorax, CHU Nantes, Nantes, France

[3]INSERM, UMR S1180, Univ Paris-Sud, Université Paris-Saclay, Châtenay-Malabry, France.

[4]PolyGene AG, Rümlang, Switzerland

* present address: Leon H Charney Division of Cardiology, New York University School of Medicine (NYU-SoM), 522 First Avenue, Smilow 805, New York, NY 10016, USA.

Short title: Type 3 long QT syndrome and $Ca^{2+}$ remodeling

Word Count: 7885

# Equal contribution

§ Co-corresponding authors, jointly directed this work

Isabelle BARÓ

*l'institut du thorax*

Inserm UMR S1087, CNRS UMR C6291

IRS-UN, 8 quai Moncousu

44007 Nantes cedex 1, France

isabelle.baro@inserm.fr

Tel. +33 228 08 01 50; Fax. +33 228 08 01 30

or Flavien CHARPENTIER

same address

E-mail: flavien.charpentier@inserm.fr
Tel. +33 228 08 01 10 64; Fax. +33 228 08 01 30

## Abstract

**Aim.** Deletion of QKP1507-1509 amino-acids in *SCN5A* gene product, the voltage-gated $Na^+$ channel Nav1.5, has been associated with a large phenotypic spectrum of type 3 long QT syndrome, conduction disorder, dilated cardiomyopathy and high incidence of sudden death. The aim of this study was to develop and characterize a novel model of type 3 long QT syndrome to study the consequences of the QKP1507-1509 deletion. **Methods and results.** We generated a knock-in mouse presenting the delQKP1510-1512 mutation (*Scn5a*$^{+/\Delta QKP}$) equivalent to human deletion. *Scn5a*$^{+/\Delta QKP}$ mice showed prolonged QT interval, conduction defects and ventricular arrhythmias at the age of 2 weeks, and, subsequently, structural defects and premature mortality. The mutation increased $Na^+$ window current and generated a late $Na^+$ current. Ventricular action potentials from *Scn5a*$^{+/\Delta QKP}$ mice were prolonged. At the age of 4 weeks, *Scn5a*$^{+/\Delta QKP}$ mice exhibited a remodeling leading to $[Ca^{2+}]_i$ transients with higher amplitude and slower kinetics, combined with enhanced SR $Ca^{2+}$ load. SERCA2 expression was not altered. However, total phospholamban expression was higher whereas the amount of $Ca^{2+}$-calmodulin-dependent kinase II (CaMKII)-dependent T17-phosphorylated form was lower, in hearts from 4-week-old mice only. This was associated with a lower activity of CaMKII and lower calmodulin expression. In addition, *Scn5a*$^{+/\Delta QKP}$ cardiomyocytes showed larger $Ca^{2+}$ waves, correlated with the presence of afterdepolarizations during action potential recording. Ranolazine partially prevented action potential and QT interval prolongation in 4-week-old *Scn5a*$^{+/\Delta QKP}$ mice and suppressed arrhythmias. **Conclusion.** The *Scn5a*$^{+/\Delta QKP}$ mouse model recapitulates the clinical phenotype of mutation carriers and provides new and unexpected insights into the pathological development of the disease in patients carrying the QKP1507-1509 deletion.

**Key words**: *Scn5a*, long QT syndrome, arrhythmias, intracellular $Ca^{2+}$ homeostasis, structural defects

## Introduction

Long QT syndrome (LQTS) is a severe disorder of cardiac electrical activity. It is caused by delayed repolarization in ventricular cardiomyocytes, which results in a prolonged QT interval on the ECG and an increased susceptibility to polymorphic ventricular tachycardia and ventricular fibrillation. Mutations in genes encoding ion channels or their accessory subunits are linked to different types of LQTS.[1] Approximately 90% of LQTS mutations are in *KCNQ1* (LQTS1), *KCNH2* (LQTS2) and *SCN5A* (LQTS3) genes. Specifically, mutations in the *SCN5A*-encoded cardiac $Na^+$ channel Nav1.5 commonly alter the fast inactivation process of the channel. Physiologically, Nav1.5 channels activate rapidly to generate a large transient inward $Na^+$ current ($I_{Na,T}$) and inactivate within a few milliseconds. This current initiates the action potential of highly polarized cardiomyocytes. Nevertheless, the $Na^+$ current also includes a much smaller sustained component, called late $Na^+$ current ($I_{Na,L}$), which remains activated during the plateau phase of the action potential. LQT3 mutations result in a marked slowing of Nav1.5 inactivation and increase of $I_{Na,L}$ that prolong the action potential.[2,3]

Deletion of amino acid residues 1507–1509 QKP, close to the first described KPQ1505-1507 deletion,[4] has been identified in two families.[5,6] This mutation is associated not only with LQTS3 but also with a broader phenotypic spectrum including conduction disorder, dilated cardiomyopathy (DCM) and a high incidence of sudden death.[6] *In vitro* experiments in an heterologous expression system revealed that QKP1507-1509 deletion induced a larger $I_{Na,L}$.[5] To characterize the effects of this deletion in a physiological environment, we generated a knock-in mouse model carrying the mouse equivalent (delQKP1510-1512; $Scn5a^{+/\Delta QKP}$ mouse) to the human QKP1507-1509 deletion. Heterozygous $Scn5a^{+/\Delta QKP}$ mice share common features with patients, including long QT interval, ventricular arrhythmias, heart failure and increased risk of sudden death at a young age. We found that the deletion induces abnormal $Ca^{2+}$ cycling correlated with secondarily decreased $Ca^{2+}$-calmodulin dependent kinase II (CaMKII) activation, most probably leading to altered expression and phosphorylation of key $Ca^{2+}$ handling proteins. This may constitute a remodeling due to the very early-observed electrical abnormalities. Acute treatment with the $I_{Na,L}$ inhibitor ranolazine partially

normalized QT interval duration and suppressed arrhythmias with no effect on conduction, suggesting that it could be appropriate to be used in patients with the QKP1507-1509 deletion.

## Methods

A full description of the methods is available in the supplementary material online.

The *Scn5a*$^{+/\Delta QKP}$ mouse model was generated in PolyGene AG facilities, according to the Swiss Federal Animal Protection Law. The experimental procedures were approved by the Cantonal Veterinary Administration, Bern, Switzerland. We used Flp/FRT-mediated targeting to delete residues 1510–1512 (QKP) in the *Scn5a* gene (see supplementary material online, methods and Figure S1). Subsequent animal experiments were performed in the animal facility of Nantes University Health Research Institute (*UTE – IRS-UN*) which has been accredited by the French Ministry of Agriculture. The experimental procedures were approved by the regional ethic committee (CEEA – Pays de la Loire, France) according to the Directive 2010/63/EU of the European Union.

***Electrocardiography.***

Six-lead ECGs were recorded on mice anesthetized with isoflurane with 25-gauge subcutaneous electrodes on a computer through an analog-digital converter (IOX 1.585, EMKA Technologies, France) for monitoring and off-line analysis (ECG Auto v3.2.0.2, EMKA Technologies). ECGs were analyzed as previously described.[7]

***Morphological and histological analysis.***

Mouse heart, lungs and liver were washed with PBS, fixed in 4% paraformaldehyde and embedded in paraffin. Five-micrometer sections were stained with haematoxylin/eosin or picrosirius red and examined with a classic light microscope.

***Patch-clamp experiments.***

Whole-cell patch-clamp technique was used to record sodium current in 4-week-old mouse cardiomyocytes (see supplementary material online for cell isolation method) using a VE-2 amplifier (Alembic Instruments, Montreal, QC, Canada). Series resistance was compensated. Activation, inactivation, recovery from inactivation and slow inactivation parameters were determined at room temperature (20-22°C) using conventional voltage-clamp protocols, from a holding potential of -120 mV and in the presence of 14 mM external $Na^+$. All current measurements were normalized using the cell capacitance. Late sodium current was measured in the presence of 140 mM external $Na^+$ as the 30 µmol/L tetrodotoxin-sensitive current at the end of a 350-ms step at -20 mV.

***Action potential recordings.***

Action potentials (AP) from left atrial and right ventricular free wall were recorded at 37 ± 0.5°C with borosilicate glass microelectrodes with 15-25-MΩ impedance when filled with 3 mol/L KCl. The preparations were superfused with a modified Tyrode solution, bubbled with 95% $O_2$-5% $CO_2$ gas mixture. Preparations were paced locally with 2-ms square wave pulses with amplitude of twice diastolic threshold. The resting potential (RP), the AP amplitude (APA), the maximum upstroke velocity of phase 0 of the AP ($dV/dt_{max}$) and the AP duration at 30% ($APD_{30}$), 50% ($APD_{50}$), 70% ($APD_{70}$) and 90% ($APD_{90}$) of full repolarization were measured under baseline conditions and after 10 min of superfusion with ranolazine (10 µmol/L; Tocris Bioscience, UK).

***Calcium imaging.***

$[Ca^{2+}]_i$ transients and $Ca^{2+}$ sparks were recorded in 4-week-old mouse cardiomyocytes (see supplementary material online for cell isolation method) loaded for 30 minutes with fluorescent $Ca^{2+}$ dye (Fluo-3 AM, 5 µmol/L) and superfused with a control solution. To record $[Ca^{2+}]_i$ transients, cells were paced at 0.5 Hz by field stimulation. Spontaneous $Ca^{2+}$ sparks were obtained in quiescent cells after $[Ca^{2+}]_i$ transients recordings. SR $Ca^{2+}$ load was estimated by rapid caffeine application. Images were obtained with confocal

microscopy. The line scan was selected parallel to the longitudinal cell axis. The fluorescence values (F) were normalized by the basal fluorescence ($F_0$) in order to obtain the fluorescence ratio ($F/F_0$).

***Western blot analysis.***

Protein samples were prepared from left ventricular free walls. Forty micrograms of proteins were separated on SDS-PAGE gels and transferred on nitrocellulose membranes. Membranes were blocked and incubated with primary antibodies targeted against Nav1.5 (D9J7S, Cell Signaling technology; 1:1000), SERCA2 (PA5-29380 Thermo Scientific; 1:2000), $Na^+/Ca^{2+}$ exchanger NCX1 (Santa Cruz Biotechnology; 1:1000), CaMKII (PA5-22168 Thermo Scientific; 1:1000), p-CaMKII (MA1-047 Thermo Scientific; 1:2000), ox-CaMKII (GTX36254 GeneTex; 1:1000), phospholamban (PLB; Santa Cruz Biotechnology; 1:1000), pPLB-T17 (Santa Cruz Biotechnology; 1:5000), pPLB-S16 (Santa Cruz Biotechnology; 1:1000), type 2 ryanodine receptor (RyR2; MA3-925 Thermo Scientific; 1:2000), pRyR2-S2808 (A010-30 Badrilla; 1:4000), pRyR2-S2814 (A010-31 Badrilla; 1:4000), pRyR2-S2030 (A010-32 Badrilla; 1:4000), N-cadherin (4061, Cell Signaling technology; 1:1000) and calmodulin (CaM; 05-173 EMD Millipore; 1:1000). In addition, an anti-GAPDH antibody (Santa-Cruz Biotechnologies; 1:10000 dilution) was used as an external/internal control. Next, membranes were incubated with the *ad hoc* secondary horseradish peroxidase (HRP) antibody (Santa Cruz; 1:10000). Incubation was followed by detection using chemiluminescence. Western-blot quantification was performed with Image Lab™ 5.2.1 software (Bio-Rad Software).

***Immunohistochemistry.***

Heart cryosections and isolated cardiomyocytes were immunostained for α-actinin 2. The samples were blocked and permeabilized before incubation with primary and secondary antibodies. Sections were mounted using ProLong Gold Antifade mountant with DAPI (Thermo Fischer Scientific) to counter-stain nuclei.

To visualize t-tubule network, freshly isolated cardiomyocytes were stained with Di-8 ANEPPS (Invitrogen). The samples were imaged with a Nikon A1 confocal microscope (objective o.i. 60x, N.A. 1.4,

Nikon) and captured with NIS-Elements software. Directional analysis of α-actinin 2 and t-tubule staining were performed with ImageJ, as described by Wagner *et al*.[8]

***Echocardiography***

Two-dimensional echocardiography was performed on mice anaesthetized with isoflurane using a Vivid 7 Dimension ultrasonography (GE Healthcare) with a 14-MHz transducer. Left ventricular diameter and free wall thickness, as well as septal thickness, were measured from long-axis images obtained by M-mode echocardiography. Systolic function was further assessed by calculation of the ejection fraction.

***Mathematical modeling of mouse ventricular action potentials***

We used the 2001 single-cell mouse model of Pandit and collaborators (http://models.cellml.org/electrophysiology). For the *Scn5a*$^{+/\Delta QKP}$ model, late current was assumed to represent 3% of the peak current[9] and both fast and slow steady-state inactivation curves were shifted by 6 mV to the depolarized potential, as experimentally observed (see figure 4C and supplementary material online, Supplemental table 1). Time constants of fast and slow inactivation, $\tau_h$ and $\tau_j$ respectively, were also modified (see figure 3D) and SERCA2 $Ca^{2+}$ flux was reduced by 3 in order to correspond to the 3-fold increase of the $[Ca^{2+}]_i$ transient decay time (see figure 5A).

***Statistics.***

Data are expressed as mean ± S.E.M. Statistical analysis was performed with Prism5 (GraphPad Software, Inc.). Significant differences were determined with Student *t*-test or Mann-Whitney U test for comparison of two groups. Wilcoxon test was used to compare paired values. Kaplan-Meier analysis and log-rank test were used to compare the survival distributions. For more than two groups, 1-way ANOVA or Kruskal-Wallis test was performed with Bonferroni or Dunn post-test when appropriate. For percentage comparison, Fisher exact test was used. A *P* value below 0.05 was considered significant.

## Results

*Scn5a*$^{+/+}$*-Flp* and *Scn5a*$^{+/\Delta QKP\text{-}neo}$ mice developed normally. Western blot analysis showed no appreciable difference in ventricular expression of Nav1.5 protein between *Scn5a*$^{+/\Delta QKP}$ mice and WT mice (supplementary material online, Figure S2). Since no parameter allowed to discriminate WT mice from *Scn5a*$^{+/+}$*-Flp* mice, we pooled these two groups in a single *Scn5a*$^{+/+}$ group (see below and supplementary material online, Figure S3).

### *Electrocardiographic phenotype and premature mortality in Scn5a*$^{+/\Delta QKP}$ *mice*

ECG was recorded at the age of 3-4 weeks in all mice studied and at 2 weeks for a subset of mice. Figure 1A depicts representative examples of ECG recordings from 2- and 4-week-old anesthetized mice in sinus rhythm. Only ~30% of 2-week-old and ~20% of 3-4-week-old *Scn5a*$^{+/\Delta QKP}$ mice were in sinus rhythm. In these mice, RR interval did not differ from that in *Scn5a*$^{+/+}$ mice at 2 (137 ± 3 ms, n = 25 for *Scn5a*$^{+/+}$ mice *versus* 141 ± 5 ms, n = 9 for *Scn5a*$^{+/\Delta QKP}$ mice) or 4 (128 ± 1 ms, n = 142 for *Scn5a*$^{+/+}$ mice *versus* 126 ± 4 ms, n = 22 for *Scn5a*$^{+/\Delta QKP}$ mice) weeks of age. However, *Scn5a*$^{+/\Delta QKP}$ mice exhibited a marked prolongation of QTc interval compared to *Scn5a*$^{+/+}$ mice. Ventricular conduction as reflected by QRS interval was also prolonged in *Scn5a*$^{+/\Delta QKP}$ mice compared to *Scn5a*$^{+/+}$ mice (Figure 1B), while atrial and atrioventricular conduction was not altered (data not shown). Most *Scn5a*$^{+/\Delta QKP}$ mice, even at the age of 2 weeks, exhibited rhythm disorders. Indeed, functional second-degree atrioventricular block (fAVB), resulting from prolonged ventricular repolarization and refractoriness, occurred in ~30% of *Scn5a*$^{+/\Delta QKP}$ mice (2/6 and 32/102 at 2 and 3-4 weeks respectively; Figure 1C). Spontaneous episodes of monomorphic and polymorphic premature ventricular beats and/or tachycardia (PVB/VT) were also observed in ~30% of 2-week-old *Scn5a*$^{+/\Delta QKP}$ mice (2/6) and ~50% of 3-4-week-old *Scn5a*$^{+/\Delta QKP}$ mice (48/102), whereas this was almost absent in *Scn5a*$^{+/+}$ mice (1/161 in 3-4-week-old *Scn5a*$^{+/+}$ mice; Figure 1C). One event of lethal ventricular fibrillation could be recorded in a 4-week-old *Scn5a*$^{+/\Delta QKP}$ mouse (Figure 1D). We failed to observe any atrial arrhythmia. In accordance with the pathology observed in patients, *Scn5a*$^{+/\Delta QKP}$ mice displayed shortened life expectancy

compared to control mice (median survival: 6.4 weeks; Figure 1E), without any difference between males and females. The number of mice exhibiting tachyarrhythmias and AVB progressively decreased with ageing, suggesting that mostly mice in sinus rhythm survived (Figure 1F).

***Abnormal cardiac function in 4-week-old Scn5a$^{+/\Delta QKP}$ mice***

Heterozygous *Scn5a*$^{+/\Delta QKP}$ offspring were born at a Mendelian frequency. At the age of 2 and 4 weeks, they presented a small but significant lower body weight compared to *Scn5a*$^{+/+}$ mice (Figure 2A-a). Four-week-old *Scn5a*$^{+/\Delta QKP}$ mice also displayed some symptoms of congestive heart failure. Morphological examination of whole hearts and longitudinal sections from *Scn5a*$^{+/\Delta QKP}$ mice indicated significantly larger left ventricular free-wall thickness compared to *Scn5a*$^{+/+}$ mice at 10 weeks of age, but not at 2 or 4 weeks (Figure 2B). At the cellular level, both α-actinin 2 and t-tubule network were disorganized at 4 but not 2 weeks of age in *Scn5a*$^{+/\Delta QKP}$ mice (supplementary material online, Figure S4). Consistently, heart weight/tibia length ratio was significantly higher in *Scn5a*$^{+/\Delta QKP}$ mice compared to *Scn5a*$^{+/+}$ mice at 4 weeks (Figure 2A-b). *Scn5a*$^{+/\Delta QKP}$ mice also exhibited cardiomyocytes hypertrophy, as indicated by their larger cell capacitance (supplementary material online, Table S1). At the same age, the echocardiography results show that both the septum and left ventricle free wall thickness was already larger, probably due to incomplete relaxation of the beating heart (supplementary material online, Figure S5). These structural alterations could be linked to altered Nav1.5 macromolecular complex, as reflected by the lower interaction of Nav1.5 with N-cadherin in 4-week old *Scn5a*$^{+/\Delta QKP}$ mice compared to *Scn5a*$^{+/+}$ mice (supplementary material online, Figure S6). In addition, the atria of *Scn5a*$^{+/\Delta QKP}$ mice frequently contained organized thrombi. Lung weight/tibia length ratio was higher in 4-week-old *Scn5a*$^{+/\Delta QKP}$ mice compared to *Scn5a*$^{+/+}$ mice but neither pulmonary congestion nor edema was observed (Figure 2C). Regarding the right ventricular dysfunction, no significant alteration of the liver weight/tibia length was detected (data not shown). However, histological analysis showed chronic congestive liver with blood stasis in the capillary vessels between centroglobular and periglobular veins in all *Scn5a*$^{+/\Delta QKP}$ mice but not in *Scn5a*$^{+/+}$ littermates (Figure 2D). Finally, a small but

significantly higher level of left ventricular fibrosis was observed in these animals compared to *Scn5a*$^{+/+}$ mice (Figure 2E).

***Occurrence of a late Na$^+$ current in Scn5a$^{+/\Delta QKP}$ mice***

Figure 3A displays representative $Na^+$ currents recorded from 4-week-old *Scn5a*$^{+/+}$ and *Scn5a*$^{+/\Delta QKP}$ cardiomyocytes. Peak current density was not affected by the QKP deletion (Figure 3B) nor was the steady-state activation voltage dependence (Figure 3C and supplementary material online, Table S1). Consistent with unchanged peak current density, the expression of Nav1.5 protein, tested by immunoblotting, showed no appreciable difference between *Scn5a*$^{+/\Delta QKP}$ and *Scn5a*$^{+/+}$ mice (supplementary material online, Figure S2). Steady-state inactivation was significantly shifted toward depolarized potentials in *Scn5a*$^{+/\Delta QKP}$ cardiomyocytes (Figure 3C and supplementary material online, Table S1). As a consequence, the window current was increased. In addition, the slow and fast time constants of inactivation were significantly higher in *Scn5a*$^{+/\Delta QKP}$ cardiomyocytes (Figure 3D). However, recovery from inactivation was similar between the two groups (supplementary material online, Figure S7 and Table S1). Finally, the TTX-sensitive late $Na^+$ current measured at the end of a 350-ms depolarizing step was much larger in *Scn5a*$^{+/\Delta QKP}$ cardiomyocytes (Figure 3E).

***Scn5a$^{+/\Delta QKP}$ mice exhibit prolonged action potentials and early afterdepolarizations***

Ventricular action potential duration (APD) was dramatically prolonged in 4-week-old *Scn5a*$^{+/\Delta QKP}$ mice (Figure 4A) at a pacing cycle length of 200 ms. *In silico* modeling showed that it may be also the case at shorter pacing cycle lengths (100 ms, Figure S8). Ventricular preparations from *Scn5a*$^{+/\Delta QKP}$ mice displayed a depolarized resting membrane potential and a lower action potential (AP) amplitude compared to *Scn5a*$^{+/+}$ mice (Figure 4B). There was also a 35%-lower $dV/dt_{max}$ in *Scn5a*$^{+/\Delta QKP}$ preparations compared to *Scn5a*$^{+/+}$ preparations (104 ± 20 V/s, n = 8, *versus* 159 ± 8 V/s, n = 8, respectively, $P < 0.05$, Student *t*-test). *Scn5a*$^{+/\Delta QKP}$ mice exhibited prolonged $APD_{30}$, $APD_{50}$, $APD_{70}$ and $APD_{90}$ with respect to *Scn5a*$^{+/+}$ mice (Figure 4C). Action potential prolongation was associated with the occurrence of early afterdepolarizations

in 9 out of 17 *Scn5a*$^{+/\Delta QKP}$ ventricular preparations but in none of the *Scn5a*$^{+/+}$ preparations (Figure 4D, see also supplementary material online, Figure S8A). Resting membrane potential was also depolarized and AP durations prolonged in left atrial *Scn5a*$^{+/\Delta QKP}$ preparations (data not shown).

***Scn5a*$^{+/\Delta QKP}$ *mutation induces abnormal calcium cycling***

In the heart, intracellular $Na^+$ concentration is a key modulator of $Ca^{2+}$ homeostasis and increased intracellular $Ca^{2+}$ concentration ($[Ca^{2+}]_i$) has been closely linked to arrhythmias.[10] We thus investigated the $[Ca^{2+}]_i$ homeostasis in ventricular cardiomyocytes of 4-week-old mice to detect any additional impairment. Figure 5A shows representative confocal line-scan images recorded from *Scn5a*$^{+/+}$ and *Scn5a*$^{+/\Delta QKP}$ cardiomyocytes that were field stimulated at 0.5 Hz. The amplitude of $[Ca^{2+}]_i$ transients was moderately higher in *Scn5a*$^{+/\Delta QKP}$ cardiomyocytes than in *Scn5a*$^{+/+}$ cardiomyocytes. They were also characterized by longer time-to-peak and decay times (Figure 5A), all together suggesting a higher sarcoplasmic reticulum (SR) load and an impairment of the $Ca^{2+}$ recycling. We also recorded $Ca^{2+}$ activity in quiescent cardiomyocytes (Figure 5B). The percentage of cardiomyocytes exhibiting spontaneous $Ca^{2+}$ waves and the frequency of $Ca^{2+}$ waves were higher in *Scn5a*$^{+/\Delta QKP}$ mice than in *Scn5a*$^{+/+}$ mice, accompanied by a faster propagation speed (139.9 ± 2.6 µm/s, n = 99 *versus* 92.7 ± 6.6 µm/s, n = 10; P< 0.001), confirming an impairment of the SR function. However, no change in $Ca^{2+}$ wave amplitude was observed (peak F/F0, 2.6 ± 0.1, n = 101 *versus* 2.7 ± 0.1, n = 10). To analyze arrhythmogenic elementary $Ca^{2+}$ release through RyR2 channels, we recorded spontaneous $Ca^{2+}$ sparks in quiescent conditions. Although the mutation had no effect on $Ca^{2+}$ spark frequency [in $s^{-1}.100\ \mu m^{-1}$, 0.3 ± 0.1 (10 *Scn5a*$^{+/\Delta QKP}$ cardiomyocytes) *versus* 0.5 ± 0.1 (20 *Scn5a*$^{+/+}$ cardiomyocytes)], $Ca^{2+}$ sparks in *Scn5a*$^{+/\Delta QKP}$ cardiomyocytes were higher (peak $F/F_0$, 2.3 ± 0.1 *versus* 1.9 ± 0.1; P< 0.01), wider (full width at half-maximum amplitude in µm, 3.1 ± 0.2 *versus* 2.0 ± 0.1; P< 0.001) and longer (full duration at half-maximum peak in ms, 47.8 ± 3.6 *versus* 35.8 ± 2.4; P< 0.01, 66 from *Scn5a*$^{+/\Delta QKP}$ cardiomyocytes *versus* 152 from *Scn5a*$^{+/+}$ cardiomyocytes).

To investigate the mechanism involved in the enhanced $[Ca^{2+}]_i$ transient amplitude and time-to-peak, we evaluated the amount of $Ca^{2+}$ stored in the SR. The *Scn5a*$^{+/\Delta QKP}$ cardiomyocytes presented higher SR $Ca^{2+}$

load (Figure 5C) without alterations of decay time of the caffeine-evoked $[Ca^{2+}]_i$ transients (4208 ± 651 ms, n = 6 *versus* 4210 ± 656 ms in *Scn5a*$^{+/+}$ mice, n = 12), indicating no modification of the sodium/calcium exchanger (NCX1) activity.

We also used the *in silico* model to further analyze the $[Ca^{2+}]_i$ homeostasis. The model predicted that the mutation leads to both higher diastolic $[Ca^{2+}]_i$ and $[Ca^{2+}]_i$ transient amplitude at 2000-ms cycle length, in agreement with the experimental results (supplementary material online, Figure S8). The model also allowed us to simulate the effects of the mutation on $Ca^{2+}$ homeostasis at more physiological cycle lengths for mice (100 and 200 ms). In these conditions, both $[Ca^{2+}]_i$ transient amplitude and diastolic $[Ca^{2+}]_i$ elevations are exacerbated even if the SR $Ca^{2+}$ load is predicted to be lower (supplementary material online, Figure S8).

***Remodeling of key $Ca^{2+}$ handling proteins in Scn5a$^{+/\Delta QKP}$ mice***

As we observed electrocardiographic and calcium cycle abnormalities in *Scn5a*$^{+/\Delta QKP}$ mice, we investigated the expression of key $Ca^{2+}$ handling proteins. As earlier suspected, NCX1 expression was similar in both groups at 4 weeks (Figure 6A). Despite lower $Ca^{2+}$ recycling kinetics, SERCA2 (Figure 6B*;* left) expression was also similar in both groups at the same age. Since SERCA2 activity is regulated by phospholamban (PLB), its expression and phosphorylation were tested by immunoblotting. Total PLB ventricular expression was significantly higher at 4 weeks. However, its CaMKII-dependent phosphorylation at Thr17 was significantly lower in *Scn5a*$^{+/\Delta QKP}$ mice compared to *Scn5a*$^{+/+}$ mice (Figure 6B; right). These alterations may underlie the prolongation of the $[Ca^{2+}]_i$ transient decay phase. The expression of the ryanodine receptor (RyR2) was not altered in *Scn5a*$^{+/\Delta QKP}$ mice. However, its level of CaMKII-dependent phosphorylation at Ser2808 was lower (Figure 6C). PKA activity is not modified in *Scn5a*$^{+/\Delta QKP}$ mice, as reflected by the similar Ser16-phosphorylated PLB (pPLB-S16) and Ser2030-phosphorylated RyR2 (pRyR2-S2030) expression compared to *Scn5a*$^{+/+}$ mice (Figure 6B and 6C).

Recent studies have linked $I_{Na,L}$ with higher activity of CaMKII.[11] As shown in Figure 6D, CaMKII ventricular expression was slightly, though significantly, higher in 2-week-old *Scn5a*$^{+/\Delta QKP}$ mice *versus*

*Scn5a*$^{+/+}$ mice. However, at the age of 4 weeks, no significant difference in CaMKII ventricular expression was observed between *Scn5a*$^{+/\Delta QKP}$ and *Scn5a*$^{+/+}$ mice. Moreover, using an antibody against phosphoThr287-CaMKII, the active form of CaMKII, we found that CaMKII autophosphorylation (T287) in *Scn5a*$^{+/\Delta QKP}$ mice was lower compared to *Scn5a*$^{+/+}$ mice at 4 weeks (Figure 6D), consistent with the lower PLB and RyR2 phosphorylation. We also observed that the level of CaMKII oxidation (Met281-282) was also lower in *Scn5a*$^{+/\Delta QKP}$ mice, confirming lower activity of CaMKII in this model. Because CaMKII autophosphorylation and oxidation first require the formation of a $Ca^{2+}$-calmodulin/CaMKII complex, we investigated the expression of calmodulin and found that it was significantly lower in 4-week-old *Scn5a*$^{+/\Delta QKP}$ mice (Figure 6E).

Most interestingly, none of the $Ca^{2+}$ handling protein expression was modified at the age of two weeks with the exception of CaMKII expression and oxidation, which were slightly higher. However, the similar levels of phosphorylated CaMKII suggest that CaMKII activity was slightly and transiently higher, when compared to *Scn5a*$^{+/+}$ mice, in 2-week-old *Scn5a*$^{+/\Delta QKP}$ mice only. Altogether, our results strongly suggest that remodeling of the $Ca^{2+}$ handling protein expression observed at 4 weeks follows the electrical abnormalities that are already present at 2 weeks of age.

***Acute pharmacological treatment of Scn5a*$^{+/\Delta QKP}$ *mice***

Beta-blockers are commonly used for treating heart failure[12] and long QT syndrome.[13] Therefore, we evaluated the effects of propranolol *in vivo*. Acute propranolol injection (0.3-1-3 mg/kg) had no effect on the incidence of arrhythmias in *Scn5a*$^{+/\Delta QKP}$ mice (Figure 7A). In contrast, acute injection of ranolazine (IP, 30 mg/kg), which inhibits $I_{Na,L}$, suppressed arrhythmias (Figure 7B) and significantly decreased QTc interval in *Scn5a*$^{+/\Delta QKP}$ mice, without affecting QRS duration (Figure 7C) or other ECG parameters (not shown). In *Scn5a*$^{+/+}$ mice, ranolazine had no effect on any ECG parameter (supplementary material online, Figure S9). *Ex vivo*, ranolazine (10 µmol/L) shortened $APD_{70}$ and $APD_{90}$ in *Scn5a*$^{+/\Delta QKP}$ mice (Figure 7D) and decreased early afterdepolarizations and even suppressed them in 2/4 preparations *versus* 4/4 under baseline condition (Figure 7E).

## Discussion

We have generated a knock-in mouse model carrying the delQKP1510-1512 mutation on *Scn5a* gene, a mutation equivalent to the *SCN5A*-delQKP1507-1509 mutation identified in LQTS3 patients.[5,6] Our study shows that 1) this model recapitulates the patients' clinical traits, *i.e.* prolonged ventricular repolarization, conduction disorders, ventricular arrhythmias, cardiac structural disorders and a high incidence of premature death; 2) the mutation-induced alterations of Nav1.5 biophysical properties partly differ from those previously reported in an heterologous expression system[5] and lead to a larger window $Na^+$ current; 3) the dysfunction of Nav1.5 leads to arrhythmias, which precede structural defects, $Ca^{2+}$ handling abnormalities and CaMKII downregulation; 4) ranolazine, an inhibitor of $I_{Na,L}$, partially normalizes repolarization of *Scn5a*$^{+/\Delta QKP}$ mice and suppresses arrhythmias.

The *SCN5A*-delQKP1507–1509 mutation was identified in two families. In the first one,[5] the variant induced a QT prolongation, bradycardia and a PR interval prolongation to borderline values but neither arrhythmias, nor structural heart disease. In the second family,[6] the phenotype was more severe with marked QT prolongation, conduction disorders, *torsades de pointes*, ventricular fibrillation and a high incidence of sudden death. In addition, the surviving mutation carriers were diagnosed with DCM. Our study shows that *Scn5a*$^{+/\Delta QKP}$ mice exhibit a similar phenotype to that of the second family, with a markedly prolonged QT interval associated with either 2:1 functional AVB or numerous episodes of ventricular tachycardia in a majority of mice. AVB was due to a particularly prolonged ventricular refractoriness, as evidenced on the ECG recordings (Figure 1C) by P waves preceding the T waves, rather than a true AV block that is localized in the AV node. In addition, the mice exhibited a longer QRS duration, most probably due lower $Na^+$ channel availability when the cardiomyocyte resting membrane potential is less polarized as shown experimentally on AP and predicted *in silico*. Moreover, this model is characterized by high mortality at young age and signs of heart failure. The high incidence of tachyarrhythmias in *Scn5a*$^{+/\Delta QKP}$ mice could account for the premature death, as supported by one recorded fatal event of ventricular fibrillation. Alternatively, cardiac

failure cannot be excluded as the mechanism of death.

Our study confirms that the mutation induces a late $Na^+$ current as previously described in a heterologous expression system.[5] But in contrast to this previous study, we did not observe a shift of steady-state activation towards positive voltages and faster recovery from inactivation. Moreover, we recorded a non-previously described shift of steady-state inactivation towards positive voltages, which is consistent with the implication of DIII-DIV loop in inactivation process[14] and responsible for a larger $Na^+$ window current. Discrepancies between heterologous expression systems and cardiomyocytes isolated from knock-in mice were previously reported,[15,16] and the mouse models appeared to be more useful to elucidate the pathophysiological mechanisms of the *SCN5A*-related diseases.

**Two phases of disease development**

*Scn5a*$^{+/\Delta QKP}$ mouse phenotype develops in two phases. The first one is mostly characterized by electrical dysfunction. Indeed at 2 weeks of age, *Scn5a*$^{+/\Delta QKP}$ mice only exhibit prolonged QT interval and ventricular arrhythmias without any detectable signs of cardiac structural defects. This phenotype can be explained by the abnormally large $I_{Na,L}$ and $Na^+$ window currents observed in *Scn5a*$^{+/\Delta QKP}$ mice, which are responsible for AP prolongation and development of early afterdepolarizations, a likely trigger for arrhythmias.[17] This is consistent with other *SCN5A* mutations involved in LQTS3.[2,18,19] Similarly, mice with cardiac-specific expression of human N1325S-*SCN5A* ($N_{1325}S$ mice ) and knock-in mice carrying *Scn5a*-delKPQ1508-1510 mutation (equivalent to human first described delKPQ1505-1507 mutation) also showed AP prolongation, EADS and spontaneous ventricular tachyarrhythmias.[20,21] In the second phase, this primary electrical defect is followed by cardiac structural defects and mechanical dysfunction, *e.g.*, cardiomyocytes and left ventricular hypertrophy, histological signs of congestive liver,[22] organized thrombi in left atrium[23] and increased lung weight, which has been also reported as a sign of heart failure in $N_{1325}S$ mice.[20] This strongly suggests that cardiac structural defects are secondary to arrhythmias. This sequence of events has been previously shown in patients with *SCN5A* p.R222Q mutation, in whom heart failure was secondary to incessant multifocal ventricular tachyarrhythmias.[24]

Cardiac hypertrophy in 10-week old *Scn5a*$^{+/\Delta QKP}$ mice is not consistent with the DCM observed in some human *SCN5A*-delQKP1507–1509 mutation carriers.[6] *Scn5a*$^{+/\Delta QKP}$ mice, if they would survive arrhythmias, may develop a DCM, but this could not have been observed due to the very shortened life expectancy of these animals. Another *SCN5A* mutation leading to the deletion of phenylalanine in position 1486 has also been identified in patients exhibiting LQTS, severe arrhythmias and reduced left ventricular function.[25] $N_{1325}S$ mice exhibit heart failure in addition to long QT interval and ventricular arrhythmias and are characterized by a marked cardiac fibrosis, which is less pronounced in our model. The age of development of the structural disease is older in $N_{1325}S$ mice and is more consistent with the age of fibrosis development in heterozygous *Scn5a* knockout (*Scn5a*$^{+/-}$) mice.[26] Thus, despite a more severe phenotype observed in *Scn5a*$^{+/\Delta QKP}$ mice compared to $N_{1325}S$ mice, the smaller amount of fibrous tissue could be explained by their young age.

**Abnormal $Ca^{2+}$ homeostasis in *Scn5a*$^{+/\Delta QKP}$ mice**

Cardiac hypertrophy and mechanical dysfunction in 4-week-old *Scn5a*$^{+/\Delta QKP}$ mice is concomitant with alterations of $Ca^{2+}$ homeostasis. Interestingly, *Scn5a*$^{+/\Delta QKP}$ mice recapitulate the alterations of expression and/or function of proteins involved in $Ca^{2+}$ homeostasis commonly found in hypertrophic cardiomyopathy. Indeed, although *Scn5a*$^{+/\Delta QKP}$ cardiomyocytes exhibited slower $[Ca^{2+}]_i$ transient decay time, evocative of a lower SERCA2 activity, they did exhibit increased $[Ca^{2+}]_i$ transient amplitude and SR $Ca^{2+}$ content.

In the heart, intracellular $Na^+$ concentration is a well-known modulator of $Ca^{2+}$ homeostasis.[10] The slowed $I_{Na}$ inactivation, without alteration of the peak current, and the larger $Na^+$ window current most likely increase the total amount of $Na^+$ entry in *Scn5a*$^{+/\Delta QKP}$ cardiomyocytes and consequently the amount of $Ca^{2+}$ by activating NCX1 reverse mode. It has been shown that during the first part of the AP, the large $Na^+$ current activates NCX1 in reverse mode, contributing to triggering $[Ca^{2+}]_i$ transient.[27,28] Thus the larger $[Ca^{2+}]_i$ transient amplitude in *Scn5a*$^{+/\Delta QKP}$ mice can be explained by larger amount of $Na^+$ entry through the $Na^+$ channel at each twitch. Alternatively, at low pacing rates, it can be due to the increased SR $Ca^{2+}$ load. But this is most unlikely at more physiological rates for mice. Indeed, computer modeling shows that

although the $[Ca^{2+}]_i$ transient is still predicted to be of higher amplitude in *Scn5a*$^{+/\Delta QKP}$ mice than in WT mice at pacing cycle lengths of 200 and 100 ms, SR $Ca^{2+}$ overload is prevented by the lower SERCA2 activity, most likely because of a lower phospholamban CaMKII-dependent phosphorylation. This is consistent with the lower M281-282 oxidation and T287 phosphorylation levels of CaMKII, observed in our model in contrast to what is observed when the late $Na^+$ current is pharmacologically induced by means of ATX-II[29,30] and to what has been shown in $N_{1325}S$ mice.[31] This is also in contrast to what is commonly observed in heart failure.[32] One explanation for this discrepancy is the down regulation of calmodulin expression in *Scn5a*$^{+/\Delta QKP}$ cardiomyocytes at 4 weeks of age. Indeed, CaMKII is canonically activated by calmodulin binding to its CaMKII binding site, which occurs when $Ca^{2+}$ binds to CaM.[33] Lower levels of calmodulin are thus expected to induce lower levels of CaMKII activation. The mechanisms of the down regulation of calmodulin is unclear but might result from an adaptation to the increased $Na^+$ and $Ca^{2+}$ influx during prolonged AP. Similarly, we did not observe any abnormal PKA activity unlike when the late $Na^+$ current is pharmacologically increased.[30] However, this is consistent with the absence of effect of β-blockers on the arrhythmias (see below).

The longer $[Ca^{2+}]_i$ transient time to peak can be ascribed to poor excitation-contraction coupling due to transverse tubule disorganization in *Scn5a*$^{+/\Delta QKP}$ mice, as observed in experimental models of hypertrophy.[34] Non-canonical roles of voltage-gated sodium channels has already been reviewed[35] and a recent study reveals the mechanisms by which Nav1.5 dysfunction can induce cardiomyopathy[36]. In link with these observations, structural remodeling could result from cytoskeletal perturbation secondary to abnormal interactions between Nav1.5 and its interacting proteins, including cytoskeletal proteins. Indeed, interaction of N-cadherin, a component of the Nav1.5 macromolecular complex, with the sodium channel is drastically lower in 4-week old *Scn5a*$^{+/\Delta QKP}$ mice. Such a disturbed Nav1.5-N-cadherin interaction has been involved in arrhythmogenic right ventricular dysplasia, another cardiomyopathy[36]. Moreover, QKP amino acids are located near the α-actinin-2 interaction site of Nav1.5,[37] and *Scn5a*$^{+/\Delta QKP}$ mice clearly show a disorganized α-actinin 2 network. Interestingly, mutations in α-actinin-2 have been previously shown to induce both hypertrophic cardiomyopathy and ventricular arrhythmias.[38]

**Ranolazine but not β-blockers suppresses spontaneous arrhythmias in *Scn5a*$^{+/\Delta QKP}$ mice**

Ranolazine is a $I_{Na,L}$ inhibitor known to reduce QTc interval, and to suppress early afterdepolarizations and *torsades de pointes*.[39] Our study shows that acute ranolazine shortens QTc and normalizes heart rhythm of 4-week-old *Scn5a*$^{+/\Delta QKP}$ mice, when cardiac remodeling has already started. In contrast to other Nav1.5 blockers, ranolazine does not affect QRS duration in *Scn5a*$^{+/\Delta QKP}$ mice. Similarly, Moss *et al.* showed that ranolazine shortens QTc interval and improves diastolic dysfunction in LQTS3 patients, without affecting ventricular conduction.[40] Moreover ranolazine may also exert an antiarrhythmic effect by inhibiting $Na^+$ overload, which would prevent $[Ca^{2+}]_i$ increase.

The recent guidelines for LQTS management indicate that β-blockers represent the first way to use for patients.[11] In our study, propranolol alone had no beneficial effects on ventricular arrhythmias, which is consistent with the fact that management of LQTS3 patients is more complex than other LQTS patients (*e.g.* LQTS1). In fact, in LQTS3 patients, bisoprolol alone has no beneficial effects, but significantly reduces arrhythmias when associated with ranolazine.[41] This effect might be directly linked to the inhibition of $I_{Na,L}$ and secondary shortening of repolarization, but also to a decrease of $Ca^{2+}$ overload as shown in *Scn5a*-delKPQ1507-1509 mutation.[42] Whether chronic treatment with ranolazine in our model could prevent remodeling of $Ca^{2+}$ handling proteins and cardiac insufficiency remains to be investigated. However, our results suggest that targeting $I_{Na\ L}$ specifically may be sufficient to limit potentially lethal arrhythmias. The main advantages of our model are the severity and the rapid onset of the disease, which should facilitate pharmacological investigations not only for deciphering the pathophysiological mechanisms of *SCN5A*-related DCM, but also for preclinical screening of new antiarrhythmic drugs or late $Na^+$ current inhibitors.

To conclude, *Scn5a*$^{+/\Delta QKP}$ mice recapitulate the clinical phenotype of patients carrying the equivalent mutation, including QT prolongation, ventricular arrhythmias and structural remodeling. Interestingly, the Nav1.5 functional defect is associated with a lower CaMKII phosphorylation. The dysfunction of Nav1.5 leads to arrhythmias, which precede structural defects and key $Ca^{2+}$ handling proteins remodeling. This

mouse model constitutes a useful tool for preclinical screening of $I_{Na,L}$ inhibitors.

## Acknowledgements

The authors wish to thank Stéphanie Lemarchand-Mindé and Valentine Prat (Inserm UMR S1087), as well as Florence Lefèbvre (Inserm UMR S1180) for their expert technical assistance. The authors also thank the staff of the animal facility (UTE IRS-UN) and of the cell and tissue imaging core facility (MicroPICell) of the *SFR François Bonamy*. UMR S1180 is member of the Labex Lermit supported by the *Agence Nationale de la Recherche* (10-LABX-33).

**Conflict of interest:** none declared.

## Funding

The research leading to these results has received funding from the European Community's Seventh Framework Programme FP7/2007-2013 under grant agreement No. HEALTH-F2-2009-241526, EUTrigTreat (IB, FC). It was also funded by the *Agence Nationale de la Recherche* [ANR-13-BSV1-0023-01 to AMG, ANR-09-GENO-003-01 to IB, ANR-12-BSV1-0013-01 to FC].

## References


1. Amin AS, Pinto YM, Wilde AAM. Long QT syndrome: beyond the causal mutation. *J Physiol (Lond)*. 2013;**591**:4125–4139.
2. Wang DW, Yazawa K, George AL, Bennett PB. Characterization of human cardiac $Na^+$ channel mutations in the congenital long QT syndrome. *Proc Nat Acad Sci*. 1996;**93**:13200–13205.
3. Kambouris NG, Nuss HB, Johns DC, Tomaselli GF, Marban E, Balser JR. Phenotypic Characterization of a Novel Long-QT Syndrome Mutation (R1623Q) in the Cardiac Sodium Channel. *Circulation*. 1998;**97**:640–644.
4. Bennett PB, Yazawa K, Makita N, George AL Jr. Molecular mechanism for an inherited cardiac arrhythmia. *Nature*. 1995;**376**:683–685.
5. Keller DI, Acharfi S, Delacrétaz E, Benammar N, Rotter M, Pfammatter JP, Fressart V, Guicheney P, Chahine M. A novel mutation in SCN5A, delQKP 1507-1509, causing long QT syndrome: role of Q1507 residue in sodium channel inactivation. *J Mol Cell Cardiol*. 2003;**35**:1513–21.
6. Shi R, Zhang Y, Yang C, Huang C, Zhou X, Qiang H, Grace AA, Huang CLH, Ma A. The cardiac sodium channel mutation delQKP 1507-1509 is associated with the expanding phenotypic spectrum of LQT3, conduction disorder, dilated cardiomyopathy, and high incidence of youth sudden death. *Europace*. 2008;**10**:1329–1335.
7. Royer A, van Veen TAB, Le Bouter S, Marionneau C, Griol-Charhbili V, Leoni A-L, Steenman M, van Rijen HVM, Demolombe S, Goddard CA, Richer C, Escoubet B, Jarry-Guichard T, Colledge WH, Gros D, de Bakker JMT, Grace AA, Escande D, Charpentier F. Mouse model of SCN5A-linked hereditary Lenègre's disease: age-related conduction slowing and myocardial fibrosis. *Circulation*. 2005;**111**:1738–1746.
8. Wagner E, Brandenburg S, Kohl T, Lehnart SE. Analysis of tubular membrane networks in cardiac myocytes from atria and ventricles. *J Vis Exp*. 2014;(**92**):e51823
9. Wang DW, Yazawa K, George AL Jr, Bennett PB. Characterization of human cardiac $Na^+$ channel

mutations in the congenital long QT syndrome. *Proc Natl Acad Sci U S A*. 1996;**93**:13200-5.

10. Despa S, Bers DM. $Na^+$ transport in the normal and failing heart - Remember the balance. *J Mol Cell Cardiol*. 2013;**61**:2–10.
11. Wagner S, Dybkova N, Rasenack ECL, Jacobshagen C, Fabritz L, Kirchhof P, Maier SKG, Zhang T, Hasenfuss G, Brown JH, Bers DM, Maier LS. $Ca^{2+}$/calmodulin-dependent protein kinase II regulates cardiac $Na^+$ channels. *J Clin Invest*. 2006;**116**:3127-3138.
12. McMurray JJV, Adamopoulos S, Anker SD, Auricchio A, Böhm M, Dickstein K, Falk V, Filippatos G, Fonseca C, Gomez-Sanchez MA, Jaarsma T, Køber L, Lip GYH, Maggioni AP, Parkhomenko A, Pieske BM, Popescu BA, Rønnevik PK, Rutten FH, Schwitter J, Seferovic P, Stepinska J, Trindade PT, Voors AA, Zannad F, Zeiher A, ESC Committee for Practice Guidelines. ESC Guidelines for the diagnosis and treatment of acute and chronic heart failure 2012: The Task Force for the Diagnosis and Treatment of Acute and Chronic Heart Failure 2012 of the European Society of Cardiology. Developed in collaboration with the Heart Failure Association (HFA) of the ESC. *Eur Heart J*. 2012;**33**:1787–1847.
13. Priori SG, Wilde AA, Horie M, Cho Y, Behr ER, Berul C, Blom N, Brugada J, Chiang C-E, Huikuri H, Kannankeril P, Krahn A, Leenhardt A, Moss A, Schwartz PJ, Shimizu W, Tomaselli G, Tracy C. HRS/EHRA/APHRS Expert Consensus Statement on the Diagnosis and Management of Patients with Inherited Primary Arrhythmia Syndromes. *Heart Rhythm*. 2013;**10**:1932–1963.
14. Ulbricht W. Sodium Channel Inactivation: Molecular Determinants and Modulation. *Physiol Rev*. 2005;**85**:1271–1301.
15. Remme CA, Verkerk AO, Nuyens D, van Ginneken ACG, van Brunschot S, Belterman CNW, Wilders R, van Roon MA, Tan HL, Wilde AAM, Carmeliet P, de Bakker JMT, Veldkamp MW, Bezzina CR. Overlap Syndrome of Cardiac Sodium Channel Disease in Mice Carrying the Equivalent Mutation of Human SCN5A-1795insD. *Circulation*. 2006;**114**:2584–2594.
16. Watanabe H, Yang T, Stroud DM, Lowe JS, Harris L, Atack TC, Wang DW, Hipkens SB, Leake B, Hall L, Kupershmidt S, Chopra N, Magnuson MA, Tanabe N, Knollmann BC, George AL, Roden DM.

Striking *In Vivo* Phenotype of a Disease-Associated Human SCN5A Mutation Producing Minimal Changes *in Vitro*. *Circulation*. 2011;**124**:1001–1011.

17. Derangeon M, Montnach J, Baró I, Charpentier F. Mouse Models of SCN5A-Related Cardiac Arrhythmias. *Front Physiol*. 2012;**3**:210.
18. Dumaine R, Wang Q, Keating MT, Hartmann HA, Schwartz PJ, Brown AM, Kirsch GE. Multiple Mechanisms of $Na^+$ Channel Linked Long-QT Syndrome. *Circ Res*. 1996;**78**:916–924.
19. Wehrens XH, Rossenbacker T, Jongbloed RJ, Gewillig M, Heidbüchel H, Doevendans PA, Vos MA, Wellens HJJ, Kass RS. A Novel mutation L619F in the cardiac Na channel SCN5A associated with long-QT syndrome (LQT3): a role for the I-II linker in inactivation gating. *Hum Mutat*. 2003;**21**:552.
20. Tian X-L, Yong SL, Wan X, Wu L, Chung MK, Tchou PJ, Rosenbaum DS, Van Wagoner DR, Kirsch GE, Wang Q. Mechanisms by which SCN5A mutation N1325S causes cardiac arrhythmias and sudden death in vivo. *Cardiovasc Res*. 2004;**61**:256–267.
21. Nuyens D, Stengl M, Dugarmaa S, Rossenbacker T, Compernolle V, Rudy Y, Smits JF, Flameng W, Clancy CE, Moons L, Vos MA, Dewerchin M, Benndorf K, Collen D, Carmeliet E, Carmeliet P. Abrupt rate accelerations or premature beats cause life-threatening arrhythmias in mice with long-QT3 syndrome. *Nat Med.* 2001;**7**:1021–1027.
22. Moller S, Bernardi M. Interactions of the heart and the liver. *Eur Heart J*. 2013;**34**:2804–2811.
23. Antos CL, Frey N, Marx SO, Reiken S, Gaburjakova M, Richardson JA, Marks AR, Olson EN. Dilated Cardiomyopathy and Sudden Death Resulting From Constitutive Activation of Protein Kinase A. *Circ Res.* 2001;**89**:997–1004.
24. Laurent G, Saal S, Amarouch MY, Béziau DM, Marsman RFJ, Faivre L, Barc J, Dina C, Bertaux G, Barthez O, Thauvin-Robinet C, Charron P, Fressart V, Maltret A, Villain E, Baron E, Mérot J, Turpault R, Coudière Y, Charpentier F, Schott J-J, Loussouarn G, Wilde AAM, Wolf J-E, Baró I, Kyndt F, Probst V. Multifocal Ectopic Purkinje-Related Premature Contractions. *J Am Coll Cardiol.* 2012;**60**:144–156.

25. Yamamura K, Muneuchi J, Uike K, Ikeda K, Inoue H, Takahata Y, Shiokawa Y, Yoshikane Y, Makiyama T, Horie M, Hara T. A novel SCN5A mutation associated with the linker between III and IV domains of Nav1.5 in a neonate with fatal long QT syndrome. *Int J Cardiol*. 2010;**145**:61–64.
26. Derangeon M, Montnach J, Cerpa CO, Jagu B, Patin J, Toumaniantz G, Girardeau A, Huang CLH, Colledge WH, Grace AA, Baró I, Charpentier F. Transforming growth factor β receptor inhibition prevents ventricular fibrosis in a mouse model of progressive cardiac conduction disease. *Cardiovasc Res.* 2017;**113**:464–74.
27. Sipido KR, Maes M, Van de Werf F. Low Efficiency of Ca2+ Entry Through the $Na^{+}$-$Ca^{2+}$ Exchanger as Trigger for $Ca^{2+}$ Release From the Sarcoplasmic Reticulum : A Comparison Between L-Type $Ca^{2+}$ Current and Reverse-Mode Na+-Ca2+ Exchange. *Circ Res.* 1997;**81**:1034–1044.
28. Bers DM. Calcium Cycling and Signaling in Cardiac Myocytes. *Annu Rev Physiol*. 2008;**70**:23–49.
29. Sag CM, Mallwitz A, Wagner S, Hartmann N, Schotola H, Fischer TH, Ungeheuer N, Herting J, Shah AM, Maier LS, Sossalla S, Unsöld B. Enhanced late INa induces proarrhythmogenic SR Ca leak in a CaMKII-dependent manner. *J Mol Cell Cardiol.* 2014;**76**:94-105.
30. Fischer TH, Herting J, Mason FE, Hartmann N, Watanabe S, Nikolaev VO, Sprenger JU, Fan P, Yao L, Popov AF, Danner BC, Schöndube F, Belardinelli L, Hasenfuss G, Maier LS, Sossalla S. Late INa increases diastolic SR-Ca2+-leak in atrial myocardium by activating PKA and CaMKII. *Cardiovasc Res.* 2015;**107(1)**:184-96.
31. Yao L, Fan P, Jiang Z, Viatchenko-Karpinski S, Wu Y, Kornyeyev D, Hirakawa R, Budas GR, Rajamani S, Shryock JC, Belardinelli L. Nav1.5-dependent persistent Na+ influx activates CaMKII in rat ventricular myocytes and N1325S mice. *Am J Physiol Cell Physiol.* 2011;**301(3)**:C577-86.
32. Luo M, Anderson ME. Mechanisms of altered Ca2+ handling in heart failure. *Circ Res.* 2013;**113(6)**:690–708.
33. Hudmon A. & Schulman H. Structure–function of the multifunctional Ca2+/calmodulin-dependent protein kinase II. *Biochem J.* 2002;**364**:593–611.

34. Bénitah J-P, Kerfant BG, Vassort G, Richard S, Gómez AM. Altered communication between L-type calcium channels and ryanodine receptors in heart failure. *Front Biosci*. 2002;**7**:e263–75.

35. Black JA, Waxman SG. Noncanonical roles of voltage-gated sodium channels. *Neuron*. 2013;**80(2)**:280-91.

36. Te Riele AS, Agullo-Pascual E, James CA, Leo-Macias A, Cerrone M, Zhang M, Lin X, Lin B, Sobreira NL, Amat-Alarcon N, Marsman RF, Murray B, Tichnell C, van der Heijden JF, Dooijes D, van Veen TA, Tandri H, Fowler SJ, Hauer RN, Tomaselli G, van den Berg MP, Taylor MR, Brun F, Sinagra G, Wilde AA, Mestroni L, Bezzina CR, Calkins H, Peter van Tintelen J, Bu L, Delmar M, Judge DP. Multilevel analyses of SCN5A mutations in arrhythmogenic right ventricular dysplasia/cardiomyopathy suggest non-canonical mechanisms for disease pathogenesis. *Cardiovasc Res.* 2017;**113(1)**:102-111.

37. Ziane R, Huang H, Moghadaszadeh B, Beggs AH, Levesque G, Chahine M. Cell Membrane Expression of Cardiac Sodium Channel Nav1.5 Is Modulated by α-Actinin-2 Interaction. *Biochemistry*. 2010;**49**:166–178.

38. Chiu C, Bagnall RD, Ingles J, Yeates L, Kennerson M, Donald JA, Jormakka M, Lind JM, Semsarian C. Mutations in Alpha-Actinin-2 Cause Hypertrophic Cardiomyopathy. *J Am Coll Cardiol.* 2010; **55**:1127–1135.

39. Antzelevitch C. Arrhythmogenic mechanisms of QT prolonging drugs: Is QT prolongation really the problem? *J Electrocardiol*. 2004;**37**:15–24.

40. Moss AJ, Zareba W, SCHWARZ KQ, Rosero S, McNitt S, Robinson JL. Ranolazine Shortens Repolarization in Patients with Sustained Inward Sodium Current Due to Type-3 Long-QT Syndrome. *J Cardiovasc Electrophysiol*. 2008;**19**:1289–1293.

41. van den Berg MP, van den Heuvel F, van Tintelen JP, Volders PGA, van Gelder IC. Successful treatment of a patient with symptomatic long QT syndrome type 3 using ranolazine combined with a beta-blocker. *Int J Cardiol*. 2014;**171**:90–92.

42. Lindegger N, Hagen BM, Marks AR, Lederer WJ, Kass RS. Diastolic transient inward current in long QT syndrome type 3 is caused by $Ca^{2+}$ overload and inhibited by ranolazine. *J Mol Cell Cardiol.* 2009;**47**:326–334.

## Figure legends

**Figure 1: Ventricular arrhythmias, long QT interval and premature mortality in *Scn5a*$^{+/\Delta QKP}$ mice.** **A**. Representative lead I ECGs of 2-week (left) and 4-week old *Scn5a*$^{+/+}$ (+/+) and *Scn5a*$^{+/\Delta QKP}$ (+/ΔQKP) mice. Scale bars, 50 ms. **B**. QTc interval and QRS complex duration in *Scn5a*$^{+/+}$ and *Scn5a*$^{+/\Delta QKP}$ mice at the age of 2 weeks ($n$ = 19 and 6, respectively) and 3-4 weeks ($n$ = 142 and 22, respectively). * $P < 0.05$, *** $P < 0.001$ (Mann-Whitney test). **C**. Top. Representative 2:1 functional atrioventricular block (fAVB) and episodes of ventricular tachycardia recorded in 2-week (left) and 4-week old *Scn5a*$^{+/\Delta QKP}$ (right) mice. Scale bars, 100 ms. Bottom. Incidence of fAVB (left) and premature ventricular beats and/or tachycardia (PVB/VT, right) at the 2 ages in *Scn5a*$^{+/+}$ and *Scn5a*$^{+/\Delta QKP}$ mice (same groups as in B). * $P < 0.05$, *** $P < 0.001$ (Fisher exact test). **D**. Representative episode of ventricular fibrillation recorded in a 4-week old *Scn5a*$^{+/\Delta QKP}$ mouse. Scale bar, 500 ms. **E**. The survival curves show a significant increase in premature mortality in *Scn5a*$^{+/\Delta QKP}$ mice ($n$ = 19) compared to *Scn5a*$^{+/+}$ mice ($n$ = 34; *** $P < 0.001$; Log-rank test). **F**. Electrophysiological follow-up of *Scn5a*$^{+/\Delta QKP}$ mice between the age of 3 and 10 weeks.

**Figure 2: Cardiac structural remodeling in *Scn5a*$^{+/\Delta QKP}$ mice. A. a.** Body weight of *Scn5a*$^{+/+}$ and *Scn5a*$^{+/\Delta QKP}$ mice at the age of 2 ($n$ = 13 and 6, respectively) and 4 weeks ($n$ = 113 and 72, respectively). * $P < 0.05$, *** $P < 0.001$ (Student t-test). **b.** Heart weight (mg) / tibia length (mm) ratio (HW/TL) of *Scn5a*$^{+/+}$ and *Scn5a*$^{+/\Delta QKP}$ mice at 2 weeks ($n$ = 13 and 6, respectively) and 4 weeks ($n$ = 11 and 13, respectively). *** $P < 0.001$ (Mann Whitney test). **B**. Top. Representative histological sections of *Scn5a*$^{+/+}$ and *Scn5a*$^{+/\Delta QKP}$ hearts at 2, 4 and 10 weeks showing left ventricular hypertrophy in 10-week old *Scn5a*$^{+/\Delta QKP}$ mice. Scale bar, 1 mm. Bottom. Mean values of right (RV) and left ventricular (LV) transversal free-wall thicknesses of 2, 4 and 10-week-old *Scn5a*$^{+/+}$ (n = 6-12) and *Scn5a*$^{+/\Delta QKP}$ (n = 4-5) mice observed by histology. * $P < 0.05$ (Mann-Whitney test). **C**. Histological sections of 4-week old *Scn5a*$^{+/+}$ and *Scn5a*$^{+/\Delta QKP}$ lungs do not show any differences (left, scale bar, 100 µm), although lung weight (mg) / tibia length (mm) ratio (LW/TL) of *Scn5a*$^{+/+}$ and *Scn5a*$^{+/\Delta QKP}$ mice at 2 weeks ($n$ = 20 and 9, respectively) and 4 weeks ($n$ = 11

and 13, respectively) indicates lung congestion at the second age. *** $P < 0.001$ (Mann Whitney test). **D**. Representative histological sections of 4-week old *Scn5a*$^{+/+}$ and *Scn5a*$^{+/\Delta QKP}$ livers show chronic congestion in *Scn5a*$^{+/\Delta QKP}$ mice with blood stasis in capillary vessels. Scale bar, 100 µm. **E.** Left. Representative left ventricular sections stained with picrosirius red from 4-week-old *Scn5a*$^{+/+}$ and *Scn5a*$^{+/\Delta QKP}$ mice. Scale bar, 100 µm. Right. Quantification of left ventricular fibrosis (mean percentage of collagen per histological section) measured in 12 *Scn5a*$^{+/+}$ and 8 *Scn5a*$^{+/\Delta QKP}$ mice. ** $P < 0.01$ (Mann Whitney test).

**Figure 3: Impaired $Na^+$ current in *Scn5a*$^{+/\Delta QKP}$ cardiomyocytes. A.** Superimposed $Na^+$ currents during depolarization to various potentials from -80 mV to +25 mV (100-ms duration, 0.2 Hz; holding potential: -120 mV) in 4-week old *Scn5a*$^{+/+}$ and *Scn5a*$^{+/\Delta QKP}$ cardiomyocytes. **B.** Current density-voltage relationships in *Scn5a*$^{+/+}$ and *Scn5a*$^{+/\Delta QKP}$ cardiomyocytes (n = 11 and 9 from 6 mice per group). **C.** Superimposed steady-state activation ($G/G_{max}$, voltage protocol as in A) and inactivation ($I/I_{max}$ at –20 mV after a 350-ms voltage prepulse, 0.2 Hz) curves of *Scn5a*$^{+/+}$ ($n$ = 11-18 from 6-10 mice) and *Scn5a*$^{+/\Delta QKP}$ ($n$ = 9 from 6 mice) $Na^+$ channels. Lines: Boltzmann fits of the data. Inset: increase of the window current in the presence of the mutation. **D.** Fast and slow inactivation kinetics of the $Na^+$ current of *Scn5a*$^{+/+}$ and *Scn5a*$^{+/\Delta QKP}$ cardiomyocytes ($n$ = 11 and 9 from 4 and 5 mice, respectively). * $P < 0.05$, ** $P < 0.01$, *** $P < 0.001$ (protocol as in A, Bonferroni test). **E.** Left. Representative late $Na^+$ currents at -20 mV obtained by subtraction of the current before and after application of 30 µmol/L tetrodotoxin (TTX) in *Scn5a*$^{+/+}$ and *Scn5a*$^{+/\Delta QKP}$ cardiomyocytes. Right. TTX-sensitive late $Na^+$ current measured at the end of a 350-ms pulse (at -20 mV) in *Scn5a*$^{+/+}$ and *Scn5a*$^{+/\Delta QKP}$ cardiomyocytes ($n$ = 6 from 5 and 3 mice, respectively). * $P < 0.05$ (Mann-Whitney test).

**Figure 4: *Scn5a*$^{+/\Delta QKP}$ mice exhibit prolonged cardiac action potentials and early after-depolarizations. A**. Representative action potentials (AP) from the right ventricle of 4-week old *Scn5a*$^{+/+}$ and *Scn5a*$^{+/\Delta QKP}$ mice recorded at a pacing cycle length of 200 ms. **B**. Resting membrane potential (RMP) and AP amplitude (APA) in *Scn5a*$^{+/+}$ and *Scn5a*$^{+/\Delta QKP}$ ventricle preparations ($n$ = 8 mice in each group).

* $P < 0.05$ (Mann-Whitney test). **C**. Ventricle AP durations at 30% ($APD_{30}$), 50% ($APD_{50}$), 70% ($APD_{70}$) and 90% ($APD_{90}$) of full repolarization in *Scn5a*$^{+/+}$ and *Scn5a*$^{+/\Delta QKP}$ ($n$ = 8 in each group). ** $P < 0.01$, *** $P < 0.001$ (Mann-Whitney test). **D.** Example of early after-depolarization (EAD) observed in a *Scn5a*$^{+/\Delta QKP}$ ventricle preparation. Right. Distribution of *Scn5a*$^{+/+}$ and *Scn5a*$^{+/\Delta QKP}$ mice exhibiting EADs or not. ** $P < 0.01$ (Fisher exact test).

**Figure 5: *Scn5a*$^{+/\Delta QKP}$ mice exhibit cardiac $Ca^{2+}$ handling defects. A.** Top. Representative line scan recordings of $[Ca^{2+}]_i$ transients in *Scn5a*$^{+/+}$ and *Scn5a*$^{+/\Delta QKP}$ cardiomyocytes. Bottom. Amplitude ($F/F_0$), time to peak and decay time of the $[Ca^{2+}]_i$ transient ($n$ = 20-21 from 4-3 mice). * $P < 0.05$, ** $P < 0.01$, *** $P < 0.001$ (Student t-test). **B.** Left. Representative line scan recordings of spontaneous $Ca^{2+}$ waves in *Scn5a*$^{+/+}$ and *Scn5a*$^{+/\Delta QKP}$ cardiomyocytes. Right. Distribution of cardiomyocytes ($n$ = 31 and 23 from 4 and 3 mice, respectively) with or without waves (top, Fisher exact test) and wave frequency (bottom, Mann-Whitney test), ** $P < 0.01$. **C.** Sarcoplasmic reticulum $Ca^{2+}$ load (SR load) in *Scn5a*$^{+/+}$ and *Scn5a*$^{+/\Delta QKP}$ cardiomyocytes ($n$ = 14 and 7 from 4 and 3 mice, respectively). ** $P < 0.01$ (Student t-test).

**Figure 6: Remodeling of cardiac $Ca^{2+}$ handling proteins between the age of 2 and 4 weeks.** Expression of (**A**) $Na^+/Ca^{2+}$ exchanger (NCX1), (**B**) sarcoplasmic $Ca^{2+}$ ATPase (SERCA2), phospholamban (PLB), Thr17-phosphorylated PLB (pPLB-T17) and Ser16-phosphorylated PLB (pPLB-S16), (**C**) ryanodine receptor (RyR2), Ser2808-phosphorylated RyR2 (pRyR2-S2808), Ser2814-phosphorylated RyR2 (pRyR-S2814) and Ser2030-phosphorylated RyR2 (pRyR2-S2030), (**D**) $Ca^{2+}$-calmodulin-dependent kinase II (CaMKII), Thr287-phosphorylated CaMKII (p-CaMKII), and oxidized-CaMKII (oxCaMKII), and (**E**) calmodulin (CaM), in 2-week and 4-week old *Scn5a*$^{+/\Delta QKP}$ heart (n = 4-10). Protein expression is expressed as ratio to glyceraldehyde-3-phosphate deshydrogenase (GAPDH) expression and normalized to its respective *Scn5a*$^{+/+}$ ratio (n = 4-14). * $P < 0.05$ (Mann-Whitney test).

**Figure 7: Acute pharmacological treatment of *Scn5a*$^{+/\Delta QKP}$ mice. A.** Left. Representative lead-I ECG at

baseline and during propranolol treatment (IP, 0.3-1-3 mg/kg). Scale bar, 500 ms. Right. Incidence of premature ventricular beats and/or ventricular tachycardia (PVB/VT) in *Scn5a*$^{+/\Delta QKP}$ mice ($n$ = 9) at baseline and during propranolol treatment. **B.** Left. Representative lead-I ECG at baseline and during ranolazine treatment (IP, 30 mg/kg). Scale bar, 500 ms. Right. Incidence of PVB/VT in *Scn5a*$^{+/\Delta QKP}$ mice at baseline and during ranolazine treatment (n = 14). * $P$ < 0.05 (Fisher exact test). **C**. QTc interval and QRS complex duration in *Scn5a*$^{+/\Delta QKP}$ mice ($n$ = 14) at baseline and during ranolazine treatment. *** $P$ < 0.001 (Wilcoxon test). **D.** Top. Representative examples of ventricular APs in *Scn5a*$^{+/\Delta QKP}$ mice at a pacing cycle length of 200 ms before (Baseline) and after 10-min superfusion of ranolazine (10 µmol/L). Bottom. APDs (as in 4C) in *Scn5a*$^{+/\Delta QKP}$ mice before and after ranolazine exposure ($n$ = 4). * $P$ < 0.05 (Wilcoxon test). **E**. Representative examples of ventricular EADs in *Scn5a*$^{+/\Delta QKP}$ mice at a pacing cycle length of 200 ms before and after ranolazine exposure.

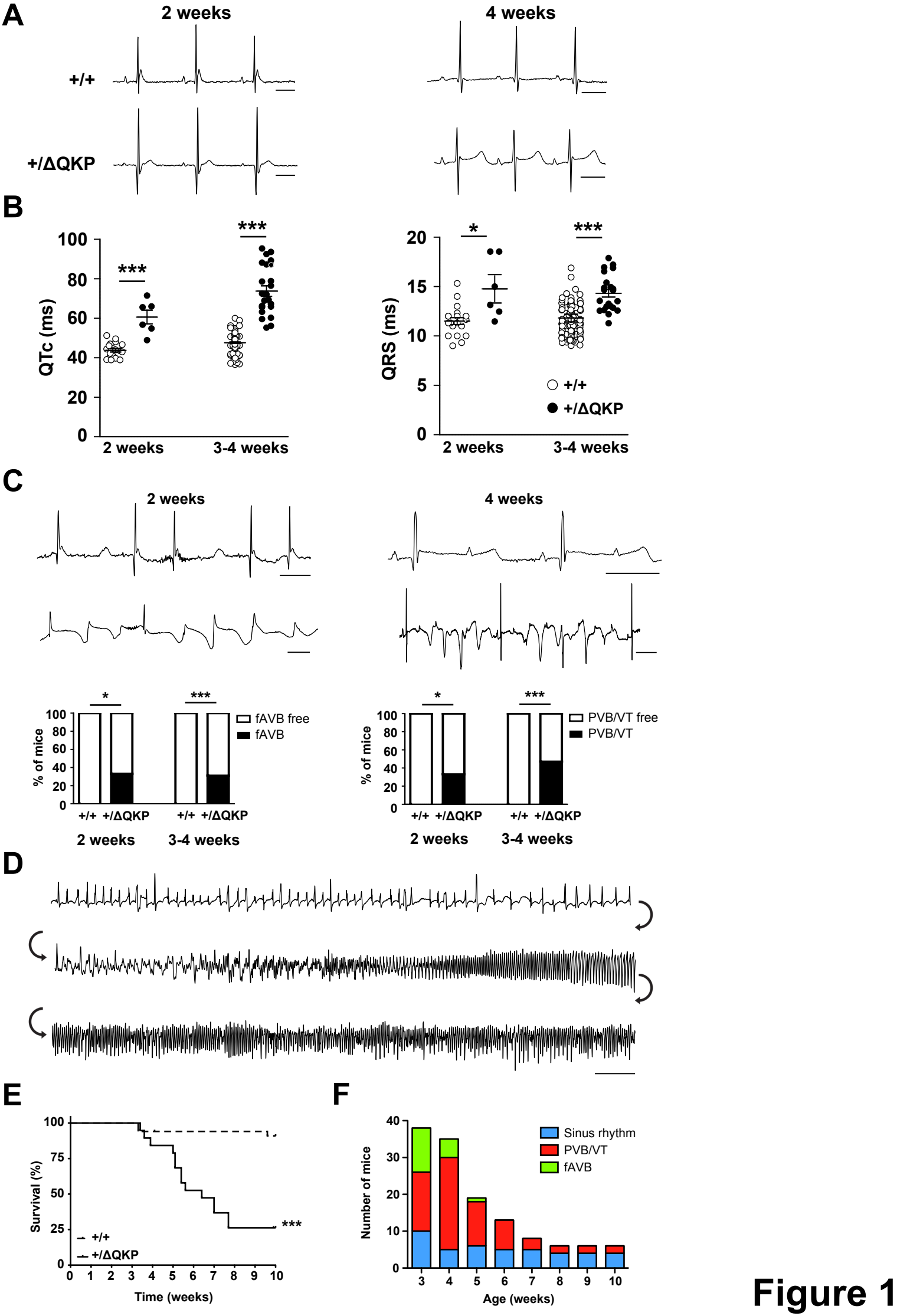
A
2 weeks
4 weeks
+/+
+/ΔQKP
B
QTc (ms)
***
***
2 weeks
3-4 weeks
QRS (ms)
*
***
+/+
+/ΔQKP
C
2 weeks
4 weeks
% of mice
fAVB free
fAVB
PVB/VT free
PVB/VT
+/+ +/ΔQKP +/+ +/ΔQKP
2 weeks
3-4 weeks
D
E
Survival (%)
+/+
+/ΔQKP
***
Time (weeks)
F
Number of mice
Sinus rhythm
PVB/VT
fAVB
Age (weeks)

**Figure 1**

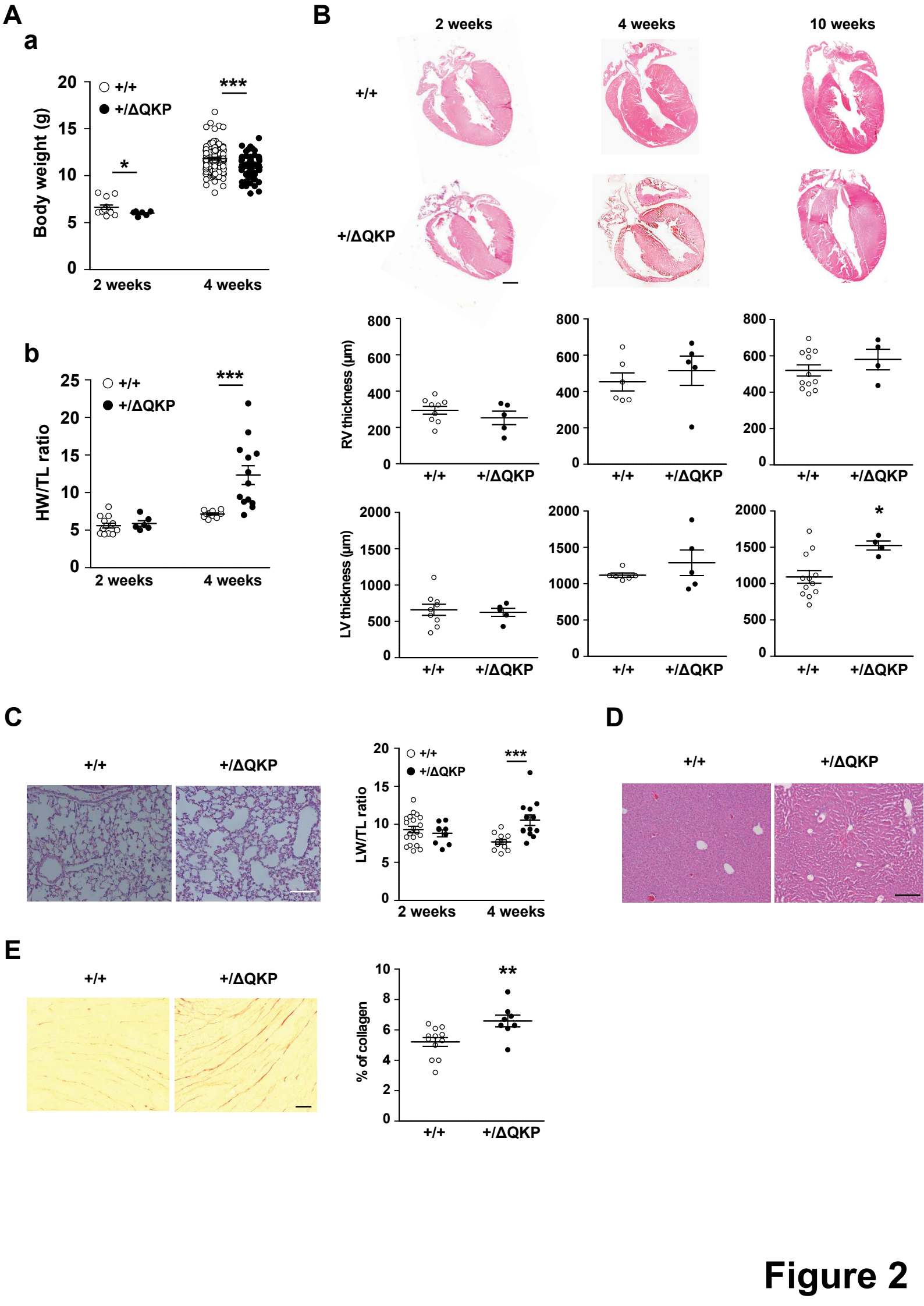
A
a
Body weight (g)
+/+
+/ΔQKP
*
***
2 weeks
4 weeks
b
HW/TL ratio
B
2 weeks
4 weeks
10 weeks
RV thickness (μm)
LV thickness (μm)
C
LW/TL ratio
D
E
% of collagen
**
Figure 2

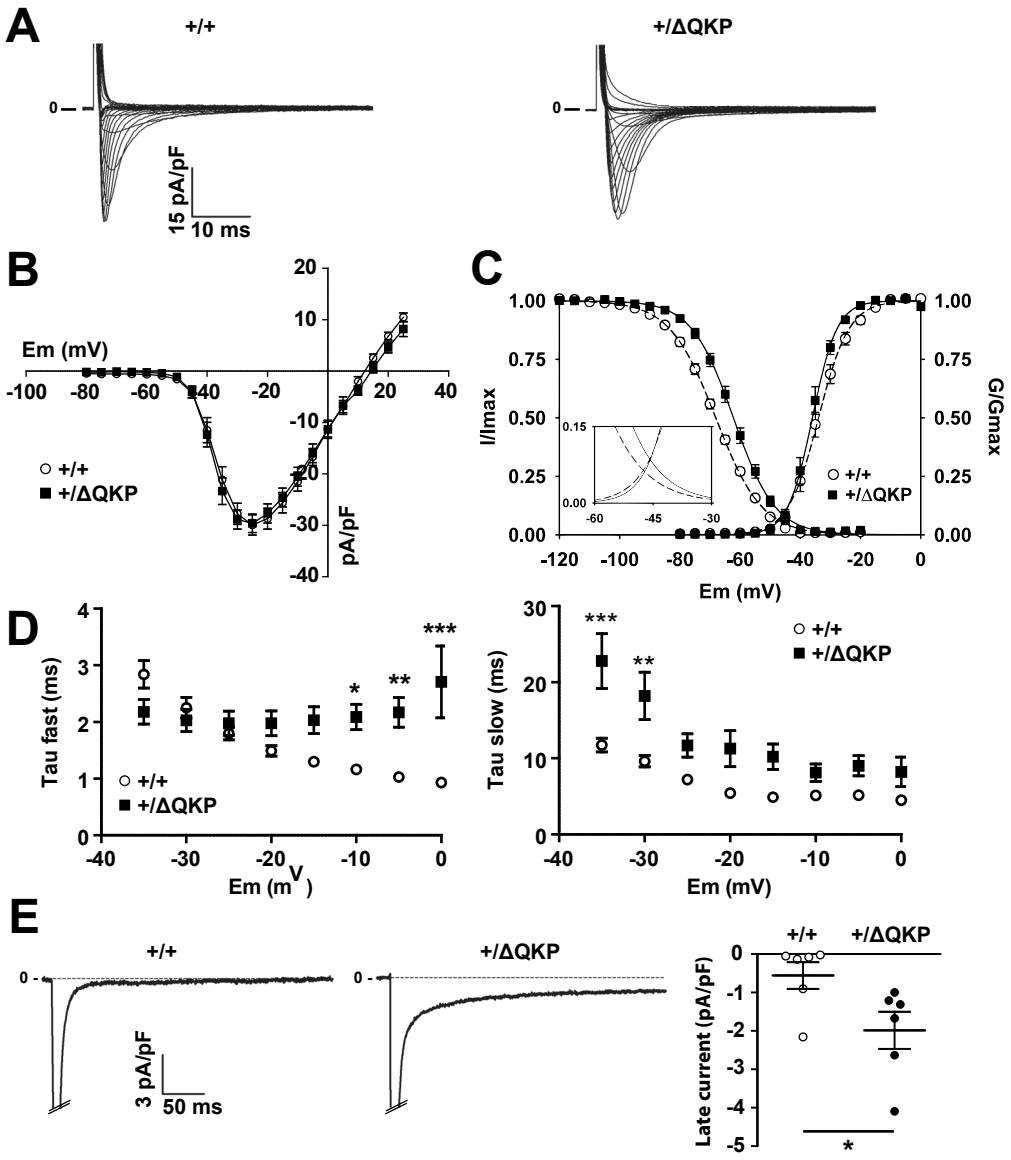
A
+/+
+/ΔQKP
0
15 pA/pF
10 ms
B
Em (mV)
-100 -80 -60 -40 -20 20 40
20 10 -10 -20 -30 -40
pA/pF
+/+
+/ΔQKP
C
I/Imax
G/Gmax
1.00 0.75 0.50 0.25 0.00
0.15
0.00
-60 -45 -30
-120 -100 -80 -60 -40 -20 0
Em (mV)
+/+
+/ΔQKP
D
Tau fast (ms)
4 3 2 1 0
-40 -30 -20 -10 0
Em (mV)
+/+
+/ΔQKP
*
**
***
Tau slow (ms)
30 20 10 0
-40 -30 -20 -10 0
Em (mV)
***
**
+/+
+/ΔQKP
E
+/+
+/ΔQKP
0
3 pA/pF
50 ms
Late current (pA/pF)
0 -1 -2 -3 -4 -5
+/+
+/ΔQKP
*

Figure 3

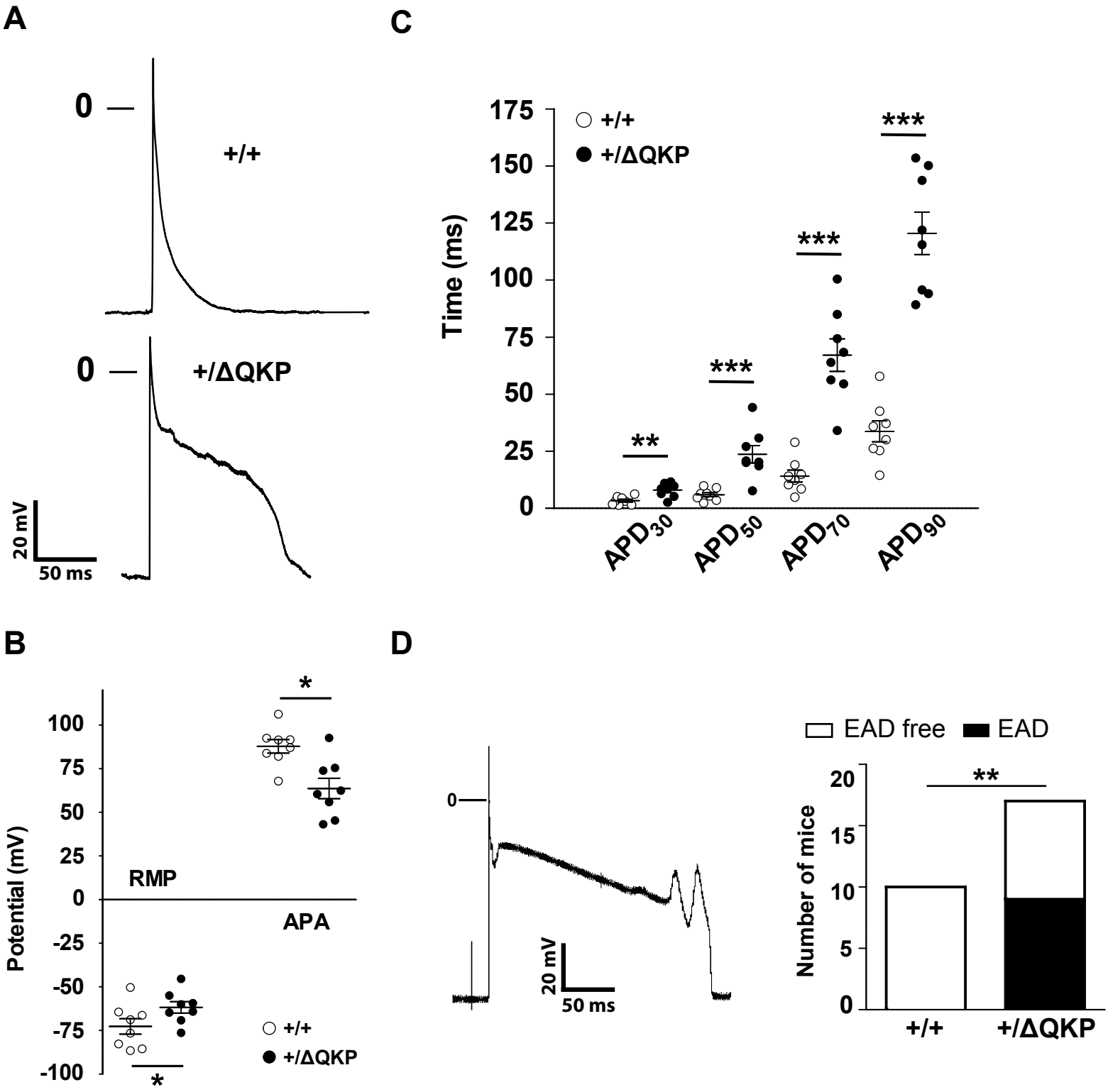
A
0
+/+
0
+/ΔQKP
20 mV
50 ms
C
+/+
+/ΔQKP
Time (ms)
175
150
125
100
75
50
25
0
**
***
***
***
APD30
APD50
APD70
APD90
B
Potential (mV)
100
75
50
25
0
-25
-50
-75
-100
RMP
APA
*
*
+/+
+/ΔQKP
D
0
20 mV
50 ms
EAD free
EAD
Number of mice
20
15
10
5
0
**
+/+
+/ΔQKP

**Figure 4**

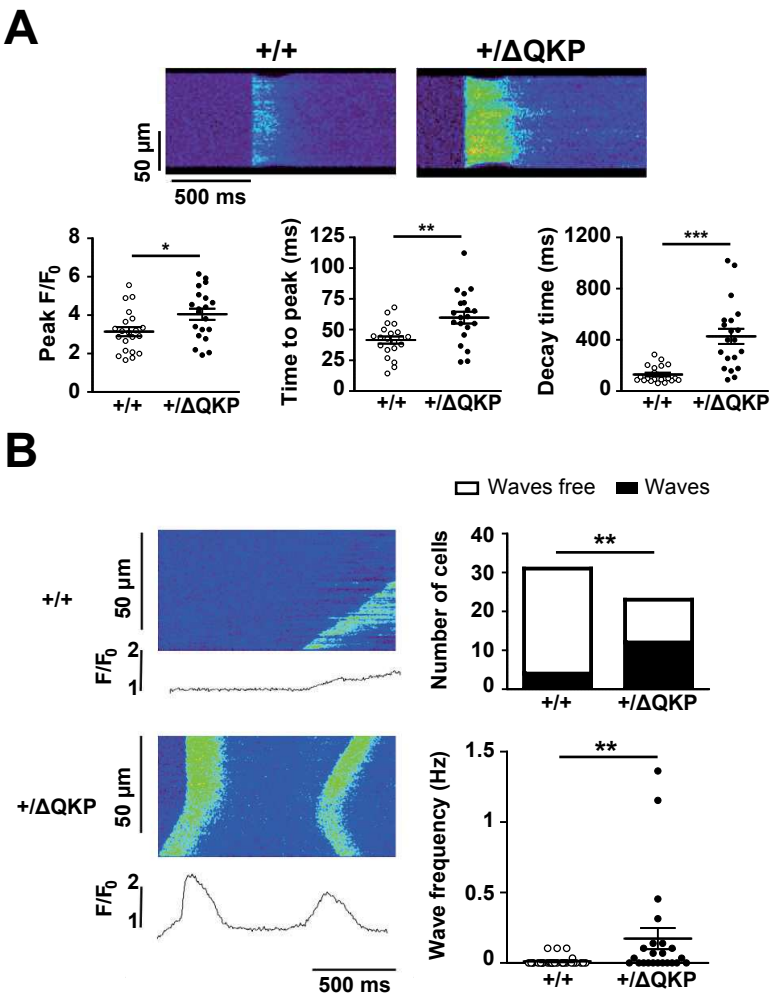
A
+/+
+/ΔQKP
50 µm
500 ms
Peak F/F0
Time to peak (ms)
Decay time (ms)
*
**
***
+/+
+/ΔQKP
B
Waves free
Waves
+/+
+/ΔQKP
50 µm
F/F0
Number of cells
Wave frequency (Hz)
500 ms
C
SR load (F/F0)

Figure 5

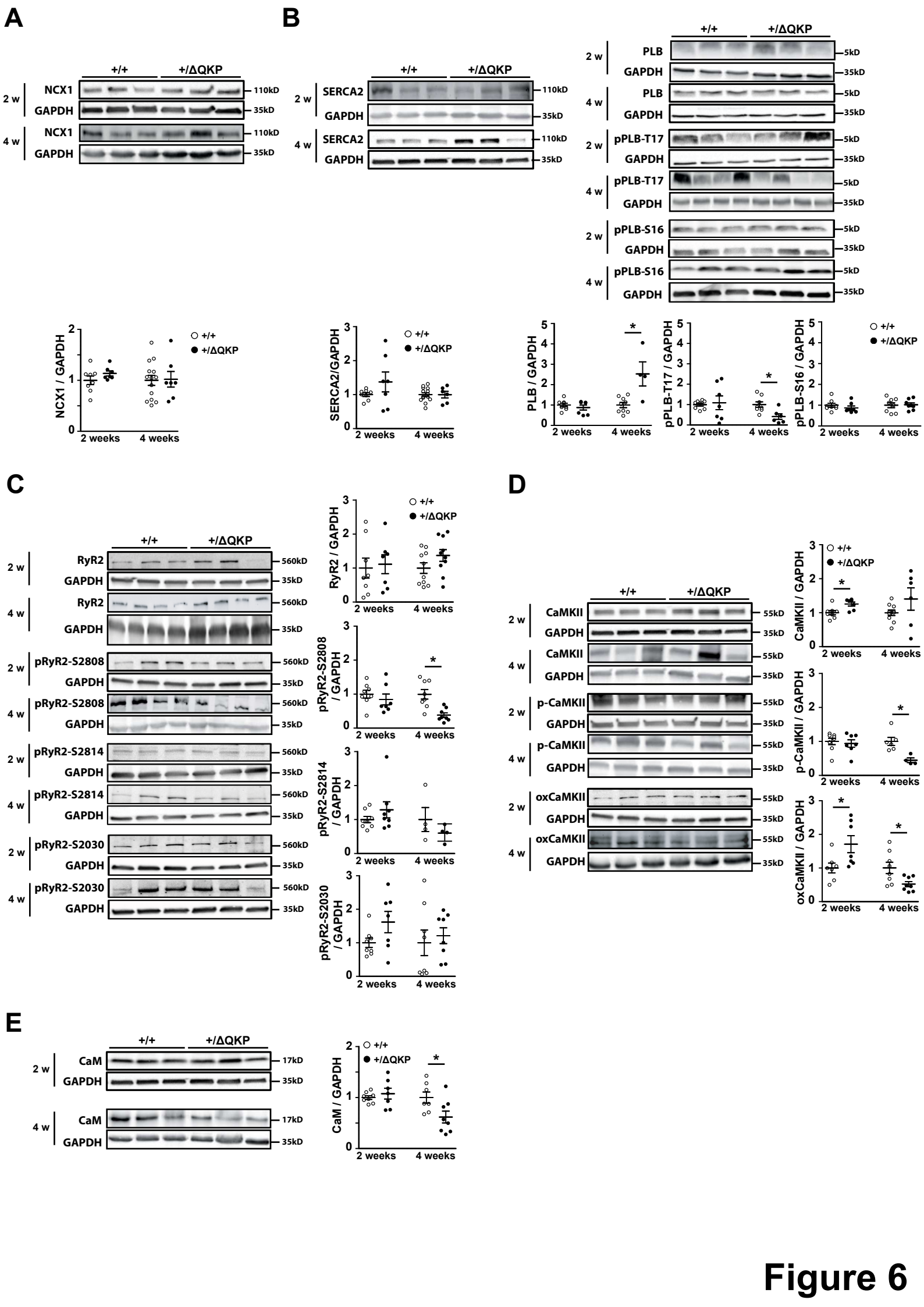
A
+/+
+/ΔQKP
2 w
NCX1
GAPDH
4 w
110kD
35kD
NCX1 / GAPDH
2 weeks
4 weeks
B
SERCA2
SERCA2/GAPDH
PLB
pPLB-T17
pPLB-S16
5kD
PLB / GAPDH
pPLB-T17 / GAPDH
pPLB-S16 / GAPDH
C
RyR2
560kD
RyR2 / GAPDH
pRyR2-S2808
pRyR2-S2808 / GAPDH
pRyR2-S2814
pRyR2-S2814 / GAPDH
pRyR2-S2030
pRyR2-S2030 / GAPDH
D
CaMKII
55kD
CaMKII / GAPDH
p-CaMKII
p-CaMKII / GAPDH
oxCaMKII
oxCaMKII / GAPDH
E
CaM
17kD
CaM / GAPDH

Figure 6

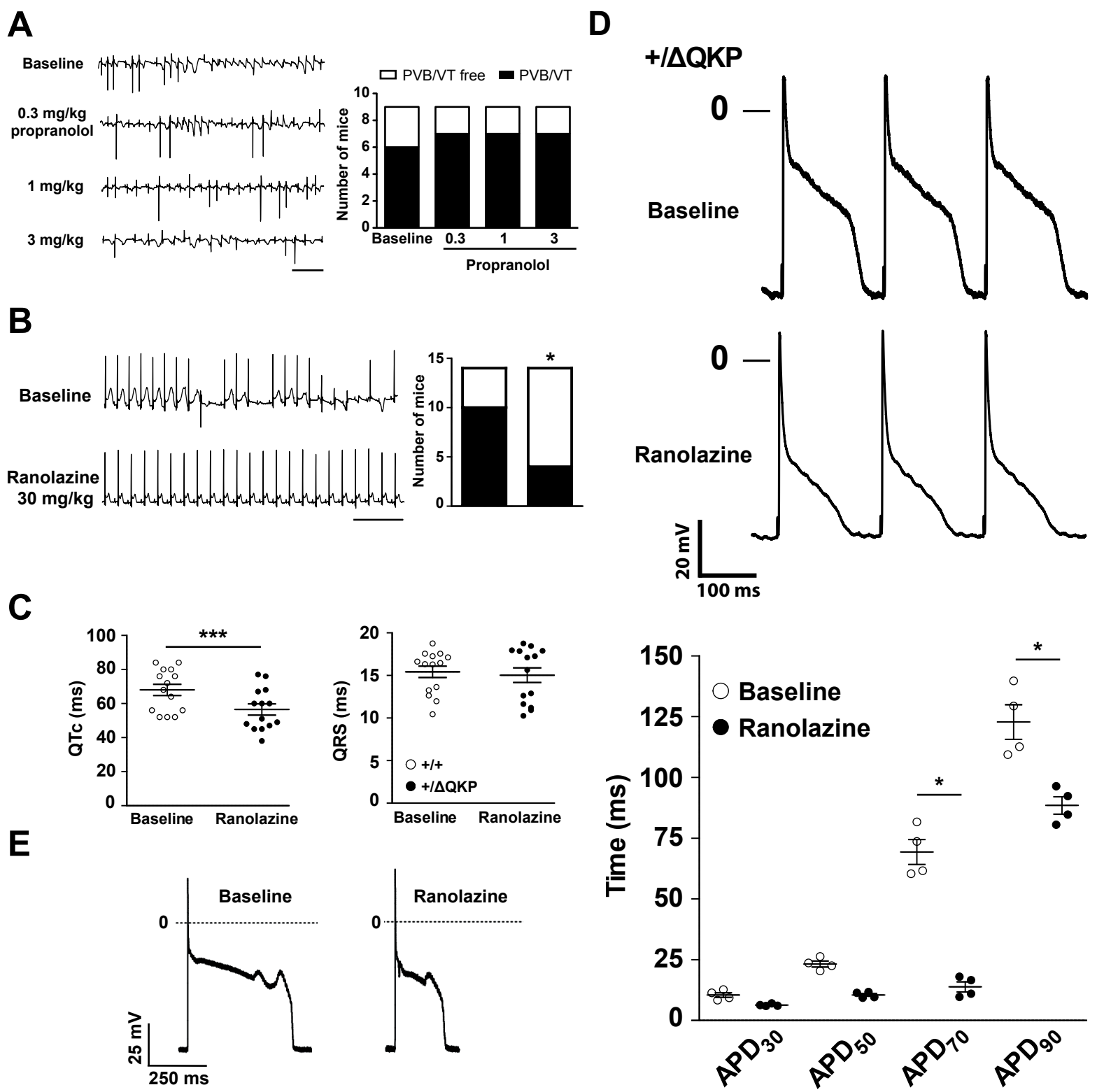
A
Baseline
0.3 mg/kg propranolol
1 mg/kg
3 mg/kg
PVB/VT free
PVB/VT
Number of mice
Baseline
0.3
1
3
Propranolol
B
Baseline
Ranolazine 30 mg/kg
Number of mice
*
C
QTc (ms)
***
Baseline
Ranolazine
QRS (ms)
+/+
+/ΔQKP
Baseline
Ranolazine
D
+/ΔQKP
0
Baseline
0
Ranolazine
20 mV
100 ms
E
Baseline
Ranolazine
0
0
25 mV
250 ms
Time (ms)
Baseline
Ranolazine
*
*
APD30
APD50
APD70
APD90

Figure 7

# Arrhythmias precede cardiomyopathy and remodeling of $Ca^{2+}$ handling proteins in a novel model of long QT syndrome

Jérôme Montnach,[1*#] Franck F. Chizelle,[1#] Nadjet Belbachir,[1] Claire Castro,[1] Linwei Li,[3] Gildas Loussouarn,[1] Gilles Toumaniantz,[1] Agnès Carcouët,[1] Anne Julia Meinzinger,[4] Doron Shmerling,[4] Jean-Pierre Benitah,[3] Ana Maria Gómez,[3] Flavien Charpentier[1,2§], Isabelle Baró[1§]

## Online supplemental material

### Supplemental methods

#### Generation of *Scn5a*$^{+/\Delta QKP}$ mice.

We used Flp/FRT-mediated targeting to delete residues 1510–1512 (QKP) in exon 26 of the *Scn5a* gene (Supplemental Figure 1A). A Scn5aΔQKP targeting vector was cloned based on a 129Sv-derived 10.6-kb BstBI/SpeI genomic subclone spanning exons 24–28. In exon 26, the nucleotides encoding QKP amino acids were deleted (CAG AAG CCC), and a silent BamHI site was introduced for screening and identification of the mutant allele. As an insertion site for the selection cassette (a neomycin resistance cassette flanked by FRT sites), a PstI restriction site 148 bp upstream of exon 26 was chosen. The neomycin cassette was inserted in counter-orientation, because of a cryptic splice site that causes mis-splicing, and consequently, a partial gene deletion or a hypomorph in the allele carrying the neo gene. 129Sv-derived embryonic stem cells harboring the deletion were injected into C57Bl/6 blastocysts. Four male chimeras were born and bred with Flp deleter mice. Agouti offspring with deleted neomycin cassette (expressing the deletion) showed a high mortality at 5-7 weeks of age, whereas offspring carrying the *Scn5a*ΔQKP allele as well as the neomycin cassette were healthy. All genotypes appeared in Mendelian rates, and the full coincidence of mortality and genotype was highly suggestive of a high linkage of morbidity with the

*Scn5a*ΔQKP allele (mortality at 31-60 days in 15/15 *Scn5a*ΔQKP F1 mice; no premature mortality in 20 $Scn5a^{+/\Delta QKP\text{-}neo}$ mice, and no premature mortality in 35 wild type offspring; another 8 wild type F1 offspring were eliminated upon weaning and screening). Therefore, all mice used in the present study resulted from mating between $Scn5a^{+/\Delta QKP\text{-}neo}$ and *Flp*-deleter mice. Mice were bred from a mixed 129Sv X C57Bl/6 background toward a C57Bl/6J background (F2 to F10 generations; most experiments performed on F4-F5 generations). Genotyping was done using the 5' GCAGCCTGAAGAGCCCTTAATG 3' (E102.8) and 5' AAGGGAGAGGCTCAGGTGAAC¬3' (E102.9) primers to identify $Scn5a^{+/+}$ and $Scn5a^{+/\Delta QKP}$ mice, and 5' GCAGCCTGAAGAGCCCTTAATG 3' and 5' GAAGGGGCCACCAAAGAACG 3' (P-#127) primers to identify $Scn5a^{+/\Delta QKP\text{-}neo}$ mice (Supplemental Figure 1B).

**Electrocardiography.**

Mice were anaesthetized with isoflurane (Abbott Laboratories, USA) for ECG recording. Anesthetic induction was achieved at 2% to 2.5% isoflurane for 2.5 to 3 min, and anesthesia was maintained at 0.8% to 1.0%. Body temperature was maintained at 37°C with a heating pad (Harvard Apparatus, USA). Six-lead ECG was recorded with 25-gauge subcutaneous electrodes on a computer through an analog-digital converter (IOX 1.585, EMKA Technologies, France) for monitoring and off-line analysis (ECG Auto v3.2.0.2, EMKA Technologies). ECGs were analyzed as previously described.[1] QT intervals were corrected for heart rate using Bazett formula modified specifically for mice, $QTc = QT/(RR/100)^{1/2}$, with QT and RR measured in ms.

**Morphological and histological analysis.**

Mice were euthanized by cervical dislocation and lungs, liver and heart were isolated. Lung weight/tibia length and heart weight/tibia length ratios were determined. Then, the heart, lungs and liver were washed with PBS, fixed in 4% paraformaldehyde and embedded in paraffin. Serial sections of 5 µm were stained with haematoxylin/eosin or picrosirius red as previously described.[2] Sections were examined with a classic light microscope (Nikon Eclipse E-600) and pictures acquired with NIS-Elements software (v4.10, Nikon,

Japan). Right and left ventricular transversal free-wall thicknesses were quantified by averaging three measurements for each heart: one close to the apex, one in the middle and one close to the base.

**Patch-clamp experiments.**

*Isolation of cardiomyocytes.* Four-week-old mice were heparinized (600 IU/kg i.p.) and killed by cervical dislocation. The heart was quickly excised and the aorta was cannulated in cold $Ca^{2+}$-free Tyrode solution containing (in mmol/L): NaCl, 135; KCl, 4; $NaH_2PO_4$, 1.2; $MgCl_2$, 1.2; glucose, 11; HEPES, 10 (pH 7.4 with NaOH), and perfused for 2 minutes in a Langendorff system (37°C) with the same solution. Then, the heart was perfused with a low-calcium solution (0.1 mmol/L) containing 0.15 mg/mL collagenase II (350 U/mg, Worthington) and 0.03 mg/mL protease XIV (4.7 U/mg, Sigma) for 7-10 minutes. Stop solution (Tyrode solution with 0.15 mmol/L $CaCl_2$) was used for 2 minutes and the digested heart was gently chopped and triturated in the same solution. Isolated cells were washed in this solution and calcium concentration was progressively increased up to 1 mmol/L after 30 min and kept in this solution at room temperature before use. Quiescent, rod-shaped cells with clear cross-striations and smooth surface were selected for current measurements.

*Electrophysiological recording.* Whole-cell patch-clamp technique was used to record sodium current. The cells were locally superfused during $I_{Na}$ recordings with solution contained (in mmol/L) NaCl, 14 or 140; CsCl, 109 or 5; $CoCl_2$, 2.5; $CaCl_2$, 1; $MgCl_2$, 2; TEA-Cl, 25; glucose, 5; HEPES, 10 and mannitol, 20; (pH 7.4 with CsOH). The pipette solution was filled with (in mmol/L): CsCl, 50; $CaCl_2$, 1; Na-pyruvate, 5; $MgCl_2$, 3; $Na_2ATP$, 2.5; gluconic acid, 70; EGTA, 10; HEPES, 10; (pH 7.2 with CsOH). pClamp software (Axon Instruments, Union City, CA, USA) and a VE-2 (Alembic Instruments, Montreal, QC, Canada) were used for recordings. Series resistance was compensated.

Data were analyzed using pClamp (Axon Instruments) and Prism5 (GraphPad Software, Inc.). Activation, inactivation, recovery from inactivation and slow inactivation parameters were determined at room temperature (20-22°C) using conventional voltage-clamp protocols, from a holding potential of -120 mV and in the presence of 14 mM external $Na^+$. All current measurements were normalized using the cell

capacitance. To quantify the voltage dependence of steady-state activation, data from individual cells were fitted with the Boltzmann function. For steady-state inactivation, a modified Boltzmann function was used:

$$I = \frac{I_{\max} - I_{\text{late}}}{\left(1 + e^{-\frac{E_{\text{pp}} - V_{\frac{1}{2}inact}}{K}}\right)} + I_{\text{late}}$$

where $I_{max}$-$I_{late}$ is the inactivating component and $I_{late}$, the non-inactivating component of the $Na^+$ current during the test-pulse.

Data for the recovery from inactivation was fitted by a 2-exponential function. Persistent sodium current was measured in the presence of 140 mM external $Na^+$ as the 30 µmol/L tetrodotoxin-sensitive current at the end of a 350-ms step at -20 mV.

**Action potential recordings.**

For these experiments, mice of either sex were used at the age of 4 weeks. After euthanasia by cervical dislocation, the heart was quickly removed and immersed in a cold modified Tyrode solution containing (in mmol/L): NaCl, 108; $NaH_2PO_4$, 1.8; $NaHCO_3$, 25; KCl, 27; $MgCl_2$, 1; $CaCl_2$, 0.6; glucose, 55 (pH 7.4 with 5% $CO_2$). After careful dissection, left atrial or right ventricular free wall was mounted in a tissue bath chamber, the endocardial surface facing up, and superfused with a modified Tyrode solution, bubbled with 95% $O_2$-5% $CO_2$ gas mixture, warmed to 37 ± 0.5°C and containing (in mmol/L): NaCl, 120; $NaHCO_3$, 27; $NaH_2PO_4$, 1.2; KCl, 5.4; $MgCl_2$, 1.2; $CaCl_2$, 1.8; glucose, 10 (pH 7.4 with 5% $CO_2$). The flow rate in the tissue chamber was 12 ml/min. Preparations were paced with 2-ms square wave pulses with amplitude of twice diastolic threshold through bipolar Teflon-coated silver electrodes. Action potentials (AP) were recorded with borosilicate glass microelectrodes (resistances 15–25 MΩ when filled with 3 mol/L KCl) coupled to a VF102 amplifier (BioLogic, France), digitized with an EMKA-converter, and displayed with iox 1.8.0.18 software (10 kHz sampling, EMKA Technologies). APs were recorded at a pacing cycle length of 200 ms. AP characteristics were measured at steady state. We measured the resting potential (RP), the AP amplitude (APA), the maximum upstroke velocity of phase 0 of the AP ($dV/dt_{max}$) and the AP duration

at 30% ($APD_{30}$), 50% ($APD_{50}$), 70% ($APD_{70}$) and 90% ($APD_{90}$) of full repolarization. This protocol was performed under baseline conditions and after 10 min of superfusion with ranolazine (Tocris Bioscience, UK) at a concentration of 10 µmol/L. This concentration was chosen on the basis of comparative pharmacological data published in mammalian heterologous expression system[3] and on *Scn5a*$^{+/\Delta KPQ}$ mice.[4]

**Calcium imaging.**

*Isolation of cardiomyocytes.* Four-week-old mice were anesthetized with intraperitoneal pentobarbital injection (150 mg/kg). The hearts were quickly excised and the aorta were cannulated in cold solution containing (in mmol/L): NaCl, 113; KCl, 4.7; $MgSO_4$, 1.2; $KH_2PO_4$, 0.6; $NaH_2PO_4$, 0.6; $NaHCO_3$, 1.6; glucose, 20; HEPES, 10; taurine, 30 (pH 7.4 with NaOH), and perfused for 4 minutes in a Langendorff system (37°C) with the same solution. Then, the heart was perfused with a low-calcium solution (0.1 mmol/L) containing Liberase (26 U/ml; TM Research Grade, Roche) for 7-10 minutes. Digested heart was gently triturated in stop solution (solution with 0.2 mmol/L $CaCl_2$ and BSA 0.5 mg/ml). Isolated cells were washed and calcium concentration was progressively increased to 1 mmol/L. Quiescent, rod-shaped cells with clear cross-striations and smooth surface were selected for current measurements. Only rod-shaped cells, quiescent when unstimulated and excitable were used for the experiments.

*Imaging*. $[Ca^{2+}]_i$ transients and $Ca^{2+}$ sparks were recorded in intact myocytes loaded for 30 minutes with fluorescent $Ca^{2+}$ dye (Fluo-3 AM, 5 µmol/L) by dissolving Fluo-3 AM (50 µg) in 100 µl of DMSO-Pluronic F-127 mixture (4:1 weight),[5] and in control perfusion solution (in mmol/L): NaCl, 140; KCl, 4; $CaCl_2$, 1.8; $MgCl_2$, 1.1; HEPES, 10; glucose, 10 (pH 7.4, with NaOH). To record $[Ca^{2+}]_i$ transients, cells were excited at 0.5 Hz by field stimulation using two parallel platinum electrodes. Spontaneous $Ca^{2+}$ sparks were obtained in quiescent cells after $[Ca^{2+}]_i$ transients recordings. SR $Ca^{2+}$ load was estimated by rapid caffeine (10 mmol/L) application, after 1 min of stimulation to reach the steady state. Images were obtained with confocal microscopy (Leica TCS SP8, objective w.i. 63x, n.a. 1.2) by scanning the cell with a white laser. Fluorescence was excited at 505 nm and emissions were collected at >510 nm. The line scan was selected parallel to the longitudinal cell axis. Image analyses were performed by homemade routines using IDL

software (Research System Inc.). Images were corrected for background fluorescence. The fluorescence values (F) were normalized by the basal fluorescence ($F_0$) in order to obtain the fluorescence ratio ($F/F_0$). $Ca^{2+}$ sparks were detected using an automated detection system[9,6] and as an amplitude of fluorescence fourfold the standard deviation of the image. This criterion limited the detection of false events while detecting most $Ca^{2+}$ sparks. Rising time was measured as the time between maximum and minimum values of the second derivative of the fluorescence transient corresponding to the $Ca^{2+}$ spark.

**Western blot analysis.**

Protein samples were prepared from left ventricular free walls. Tissues were snap-frozen in liquid nitrogen, homogenized in ice-cold lysis buffer containing (in mmol/L): NaCl, 100, Tris-HCl, 50, EGTA, 2, $Na_3VO_4$, 2, 1% NP40 and protease inhibitors (pH 7.5 with NaOH) and centrifuged at 14000 x g for 15 minutes. Forty micrograms of proteins were separated on SDS-PAGE gels (4-15% Mini-PROTEAN® TGX Stain-Free™ Precast Gels, Bio-Rad, France) and transferred on nitrocellulose membranes (Trans-Blot® Turbo™ Nitrocellulose Transfer Packs, Bio-Rad, France). Membranes were blocked and incubated with primary antibodies targeted against Nav1.5 (D9J7S, Cell Signaling technology; 1:1000), SERCA2 (PA5-29380 Thermo Scientific; 1:2000), $Na^+/Ca^{2+}$ exchanger NCX1 (Santa Cruz Biotechnology; 1:1000), CaMKII (PA5-22168 Thermo Scientific; 1:1000), p-CaMKII (MA1-047 Thermo Scientific; 1:2000), ox-CaMKII (GTX36254 GeneTex; 1:1000), phospholamban (PLB; Santa Cruz Biotechnology; 1:1000), pPLB-T17 (Santa Cruz Biotechnology; 1:5000), pPLB-S16 (Santa Cruz Biotechnology; 1:1000), type 2 ryanodine receptor (RyR2; MA3-925 Thermo Scientific; 1:2000), pRyR2-S2808 (A010-30 Badrilla; 1:4000), pRyR2-S2814 (A010-31 Badrilla; 1:4000), pRyR2-S2030 (A010-32 Badrilla; 1:4000), N-cadherin (4061, Cell Signaling technology; 1:1000) and calmodulin (CaM; 05-173 EMD Millipore; 1:1000). In addition, an anti-GAPDH antibody (Santa-Cruz Biotechnologies; 1:10000 dilution) was used as an external/internal control. Next, membranes were incubated with the *ad hoc* secondary horseradish peroxidase (HRP) antibody (Santa Cruz; 1:10000). Incubation was followed by detection using chemiluminescence (ECL™ Prime Western

Blotting Detection Reagent, GE Healthcare Amersham™, UK). Western-blot quantification was performed with Image Lab™ 5.2.1 software (Bio-Rad Software).

**Acute pharmacological treatments.**

For these experiments, *Scn5a*$^{+/\Delta QKP}$ mice were used at the age of 3 weeks. Baseline ECG was recorded for 2 min before intraperitoneal (IP) injection of ranolazine (30 mg/kg)[7] or propranolol (0.3-1-3 mg/kg) and measurements were acquired for 10 min post-drug administration. Maximum effect on ECG parameters was measured and compared to ECG parameters before drug administration.

**Immunohistochemistry.**

Six µm-width heart cryosections and isolated cardiomyocytes were immunostained for α-actinin 2 using monoclonal antibody (clone EA-53, Sigma Aldrich) and Alexa Fluor 488 goat anti-mouse antibody IgG (Invitrogen). To realize cryosections, the hearts were removed, immediately snap-frozen in isopentane and conserved at -80°C until sections were included in Tissue-Tek OCT compound (Sakura) and cut. Heart sections were fixed in cold acetone for 10 minutes while isolated cells were fixed in 4% paraformaldehyde. The samples were put on slides, and then blocked and permeabilized in a solution containing 1% BSA, 0.5% X100 Triton and 10% normal goat serum for 30 minutes at room temperature. The slides were incubated with primary antibody (1/200) for 2 hours, washed three times with PBS and then incubated with secondary antibody (1/200) for 45 minutes at room temperature. After three 5-minute washes, slides were mounted using ProLong Gold Antifade mountant with DAPI (Thermo Fischer Scientific) to counter-stain nuclei.

To visualize t-tubules network, freshly isolated cardiomyocytes were put on 8-well Ibidi microslides, incubated with 10 µM Di-8 ANEPPS (Invitrogen) in the dark at room temperature, and washed three times before observation.

The samples were imaged with a Nikon A1 confocal microscope (objective o.i. 60x, N.A. 1.4, Nikon, France) and captured with NIS-Elements software.

Directional analysis of α-actinin 2 and t-tubules staining were performed with ImageJ, as described by Wagner *et al.*[8] Percentage of α-actinin 2 or t-tubules oriented between -45° and 135° were quantified by using cell longitudinal axis as reference. Transversal/longitudinal ratios were measured by considering as transversal or longitudinal the staining oriented between 80° and 100° and -10° and 10° respectively.

**Echocardiography**

Two-dimensional echocardiography was performed on mice using a Vivid 7 Dimension ultrasonography (GE Healthcare) with a 14-MHz transducer. Mice were anaesthetized with isoflurane (Abbott Laboratories, USA). Anesthetic induction was achieved at 5% isoflurane for 2.5 to 3 min, and anesthesia was maintained at 2.5%. In order to observe a possible structural remodeling, left ventricular diameter and free wall thickness, as well as septal thickness, were measured from long-axis images obtained by M-mode echocardiography. Systolic function was further assessed by calculation of the ejection fraction.

**Mathematical modeling of mouse ventricular action potentials - Single-cell model**

We used the 2001 mouse model of Pandit and collaborators[9]. All the equations are found in the website, only the model modifications are shown here. On the *Scn5a*$^{+/+}$ model, $G_{Na}$ was increased from 1.064 to 2 µS to obtain a $dV/dt_{max}$ of around 100 V/sec. Stimulation was shortened from 5 ms to 1 ms and its amplitude was increased from -0.6 to -3 nA to keep the same amount of injected charges. The model was run using OpenCell. Maximum step size was 0.001 s. For the *Scn5a*$^{+/\Delta QKP}$ model, the late $Na^+$ current (when fast inactivation is complete) represented 3% of the peak current[10] and both fast and slow steady-state inactivation curves were shifted by 6 mV to the depolarized potential, as observed in figure 3:

Slow inactivation:

$$h_\infty = \frac{1 - \mathbf{0.03}}{1 + e^{\left(\frac{V_m + 76.1 - \mathbf{6}}{6.07}\right)}} + \mathbf{0.03}$$

Fast inactivation:

$$j_{\infty} = \frac{1}{1 + e^{\left(\frac{V_m + 76.1 - \mathbf{6}}{6.07}\right)}}$$

From figure 3 also, time constant of fast inactivation, $\tau_h$ is voltage independent between -35 and 0 mV and corresponds to the ***Scn5a***$^{+/+}$ value at -25 mV:

$\tau_h = \mathbf{0.00210502}$ if $V_m$ > -40 mV, else $\tau_h$ equation as for ***Scn5a***$^{+/+}$.

Time constant of slow inactivation, $\tau_j$ is twice as much in the ***Scn5a***$^{+/+}$ model if $V_m$ > -40 mV:

$\tau_j = \mathbf{2} \times (0.01163 \frac{\left(1 + e^{-0.1\,(V_m + 32)}\right)}{e^{-2.535 \times 10^{-7} V_m}})$, else $\tau_j$ equation as for ***Scn5a***$^{+/+}$.

In addition, SERCA2 $Ca^{2+}$ flux was reduced by 3 in order to correspond to the 3-time increase of the $[Ca^{2+}]_i$ transient decay time (see figure 5A), as following:

$$J_{up} = {}^{\mathbf{1}}/_{\mathbf{3}} \times K_{SR} \frac{v_{maxf} f_b - v_{maxr} r_b}{1 + f_b + r_b}$$

See Pandit *et al.*[11], for variables and constants definitions.

**Immunoprecipitations of Nav1.5 channel complexes**

Flash-frozen left ventricles from *Scn5a*$^{+/+}$ and *Scn5a*$^{+/\Delta QKP}$ mice were homogenized in ice-cold lysis buffer containing (in mmol/L): NaCl, 100, Tris-HCl, 50, EGTA, 2, $Na_3VO_4$, 2, 1% NP40 and protease inhibitors (pH 7.5 with NaOH). Prior to the immunoprecipitation, 2 µg of Nav1.5 antibodies (rαNav1.5, Cell Signalling, D9J7S) were cross-linked to 25 µl of protein G-magnetic beads. After a 20-minute rotation at 4°C, 2 mg of ventricular soluble protein fractions and antibody-coupled beads were mixed for 2 hours at 4°C. Magnetic beads were then collected and washed rapidly four times with ice-cold lysis buffer, and isolated protein complexes were eluted from the beads in a mix containing NuPAGE sample reducing agent and NuPAGE LDS sample buffer (1X) at 99°C for 10 minutes. Western blots were then realized as described above on immunoprecipitated fractions and total lysates.

**Supplemental table 1: Effects of QKP deletion on sodium channel biophysical parameters.**

| | cell capacitance | current density | activation | | inactivation | | recovery from inactivation | | |
|---|---|---|---|---|---|---|---|---|---|
| | (pF) | late at –20 mV (pA/pF) | $V_{1/2}$ (mV) | K (mV) | $V_{1/2}$ (mV) | K (mV) | $A_{fast}$ (%) | $\tau_{fast}$ (ms) | $\tau_{slow}$ (ms) |
| ***Scn5a*$^{+/+}$** | 136.4±7.9 (23) | –0.6±0.3 (6) | –33.9±1.0 (11) | 4.6±0.1 (11) | –68.2±0.7 (18) | –7.5±0.3 (18) | 83.7±1.4 (11) | 3.3±0.4 (11) | 43.4±8.4 (11) |
| ***Scn5a*$^{+/\Delta QKP}$** | 238.3±13.5*** (13) | –2.0±0.5* (6) | –35.3±1.1 (9) | 3.9±0.2** (9) | –62.3±1.0*** (9) | –6.7±0.2 (9) | 77.0±2.9 (5) | 3.0±0.2 (5) | 30.3±2.2 (5) |

$V_{1/2}$ and K; voltage for half-activation or -inactivation of the $Na^+$ current and slope of steady-state activation and inactivation curves, respectively; $A_{fast}$ and $\tau_{fast}$: coefficient and time constant, respectively, of the fast component of reactivation kinetics, $\tau_{slow}$: time constant of the slow component. (n): number of cells; * P< 0.05; ** P< 0.01; *** P< 0.001 *vs.* *Scn5a*$^{+/+}$ (Mann-Whitney test).

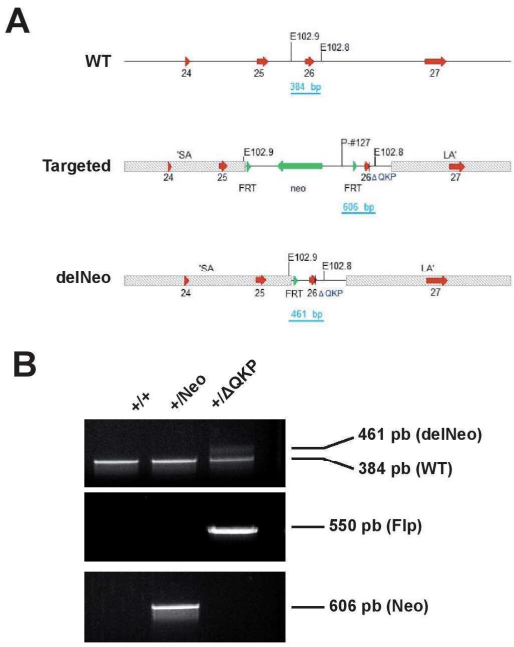


**Supplemental figure 1: generation of *Scn5a*$^{+/\Delta QKP}$ mice**. **A.** Scheme of the different alleles of the *Scn5a* locus. For selection of homologously recombined ES cells, an FRT-flanked neomycin resistance cassette (green) was used. After Flp mediated recombination (delNeo, lower panel), the neomycin resistance cassette was excised, leaving a single FRT site upstream of exon 26. The primer binding sites used for genotyping are indicated in black, and the resulting PCR products in light blue bars. **B**. PCR screening of *Scn5a*$^{+/+}$, *Scn5a*$^{+/\Delta QKP\text{-neo}}$ and *Scn5a*$^{+/\Delta QKP}$ mice.

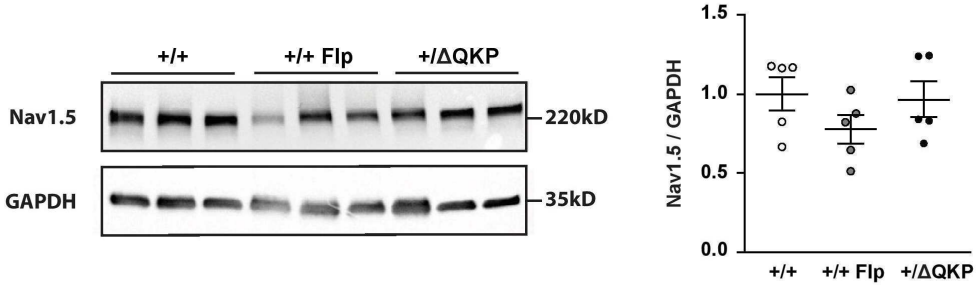


**Supplemental figure 2: expression of cardiac Nav1.5.** Nav1.5 expression in *Scn5a*$^{+/+}$, *Scn5a*$^{+/+}$*-Flp*, *Scn5a*$^{+/\Delta QKP\text{-neo}}$ and *Scn5a*$^{+/\Delta QKP}$ hearts. Protein level expressed as ratio to glyceraldehyde-3-phosphate deshydrogenase (GAPDH) expression and normalized to the *Scn5a*$^{+/+}$ ratio (n = 4-5 in each group). * $P < 0.05$ *versus* WT (Kruskal-Wallis test).

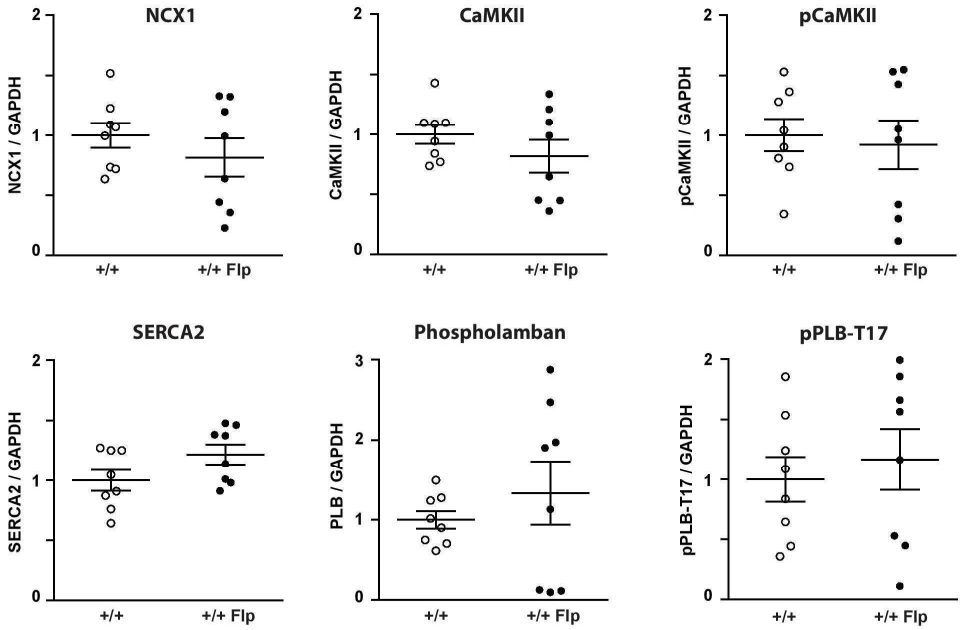


**Supplemental figure 3: similar ventricle $Ca^{2+}$ handling protein expression in *Scn5a*$^{+/+}$and *Scn5a*$^{+/+}$-*Flp* mice.** Expression of $Na^+/Ca^{2+}$ exchanger (NCX1), $Ca^{2+}$-calmodulin-dependent kinase II (CaMKII), phosphoThr-287 CaMKII (pCaMKII), sarcoplasmic $Ca^{2+}$ ATPase (SERCA2), phospholamban (PLB), and Thr17-phosphorylated PLB (pPLB-T17) in *Scn5a*$^{+/+}$-*Flp* heart. Protein expression is expressed as ratio to glyceraldehyde-3-phosphate deshydrogenase (GAPDH) expression and normalized to its respective *Scn5a*$^{+/+}$ ratio (n = 8 in each group).

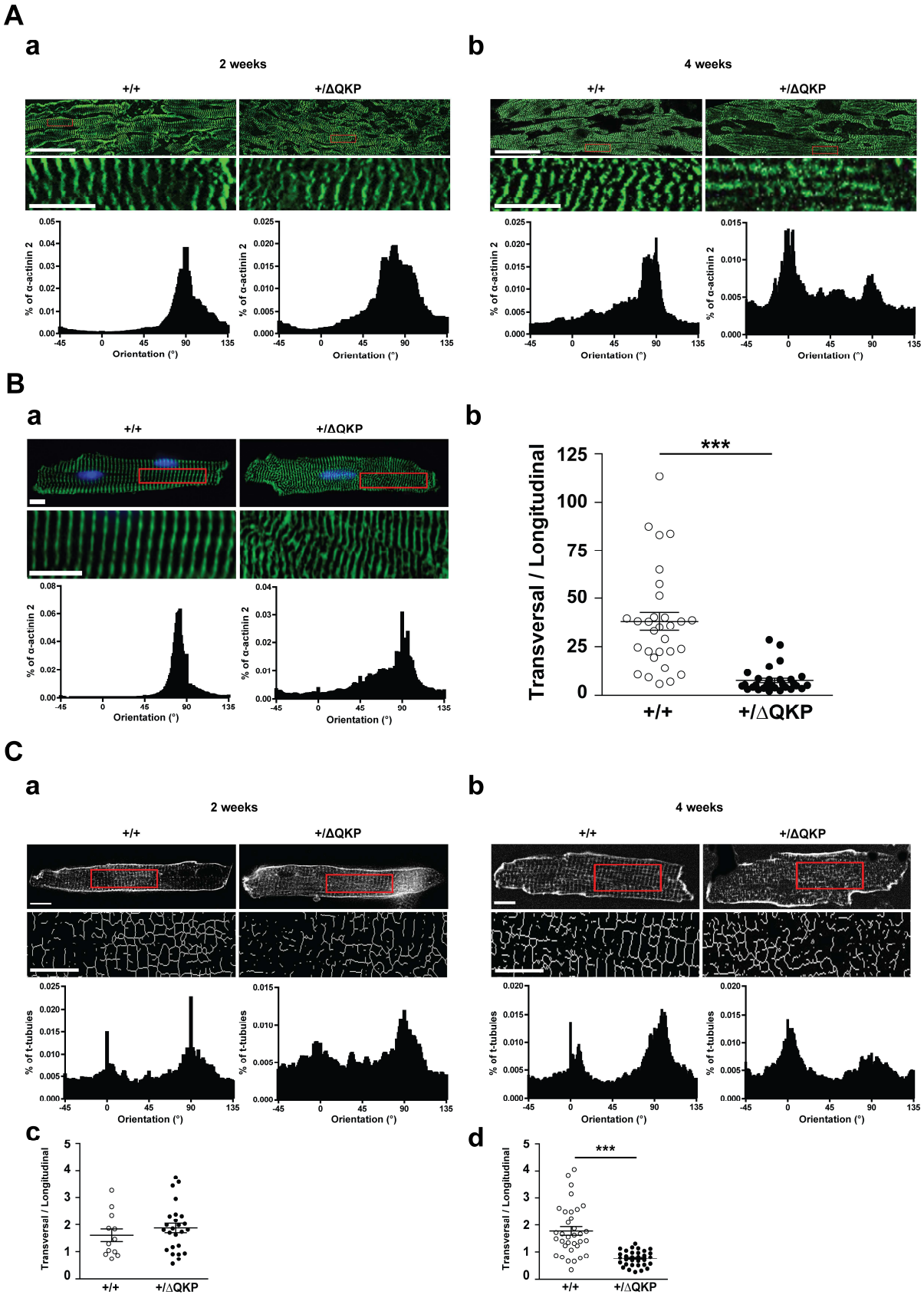
A
a
2 weeks
+/+
+/ΔQKP
% of α-actinin 2
Orientation (°)
b
4 weeks
+/+
+/ΔQKP
% of α-actinin 2
Orientation (°)
B
a
+/+
+/ΔQKP
% of α-actinin 2
Orientation (°)
b
Transversal / Longitudinal
***
+/+
+/ΔQKP
C
a
2 weeks
+/+
+/ΔQKP
% of t-tubules
Orientation (°)
b
4 weeks
+/+
+/ΔQKP
% of t-tubules
Orientation (°)
c
Transversal / Longitudinal
+/+
+/ΔQKP
d
Transversal / Longitudinal
***
+/+
+/ΔQKP

**Supplemental figure 4: α-actinin 2 and t-tubule networks are disorganized in 4- but not 2-week-old *Scn5a*$^{+/\Delta QKP}$ mice. A.** Top: Representative α-actinin 2 (green) immunostained histological sections from 2-week-old (**a**) and 4-week-old (**b**) *Scn5a*$^{+/+}$ (left) and *Scn5a*$^{+/\Delta QKP}$ mice (right). Scale bars = 75 µm. Bottom: zoom of the red frames and corresponding graphs showing the percentages of α-actinin 2 oriented between -45° and 135° compared to longitudinal cell axis. Scale bars = 10 µm. **B.** (**a**) Top: Representative α-actinin 2 immunostained cardiomyocytes isolated from 4-week-old *Scn5a*$^{+/+}$ (left) and *Scn5a*$^{+/\Delta QKP}$ mice (right). Nuclei are stained in blue. Bottom: zoom of the red frames and corresponding graphs showing the percentages of α-actinin 2 oriented between -45° and 135° compared to longitudinal cell axis. Scale bars, 10 µm. (**b**) Transversal / longitudinal ratio of α-actinin 2 fibers compared to longitudinal cell axis measured on 30 cardiomyocytes from 3 different mice in each group. *** $P < 0.001$ (Student t-test). **C.** Top: representative di-8-ANEPPS-stained cardiomyocytes isolated from 2-week-old (**a**) and 4-week-old (**b**) *Scn5a*$^{+/+}$ (left) and *Scn5a*$^{+/\Delta QKP}$ mice (right). Scale bars, 10 µm. Bottom: zoom of the red frames and graphs showing the percentages of t-tubules oriented between -45° and 135° compared to longitudinal cell axis. Scale bars, 7.5 µm. Transversal / longitudinal ratio of t-tubules compared to longitudinal cell axis measured on 25-38 cardiomyocytes from 2-week-old (**c**) and 4-week-old (**d**) mice (3 mice per group). *** $P< 0.001$ (Student t-test).

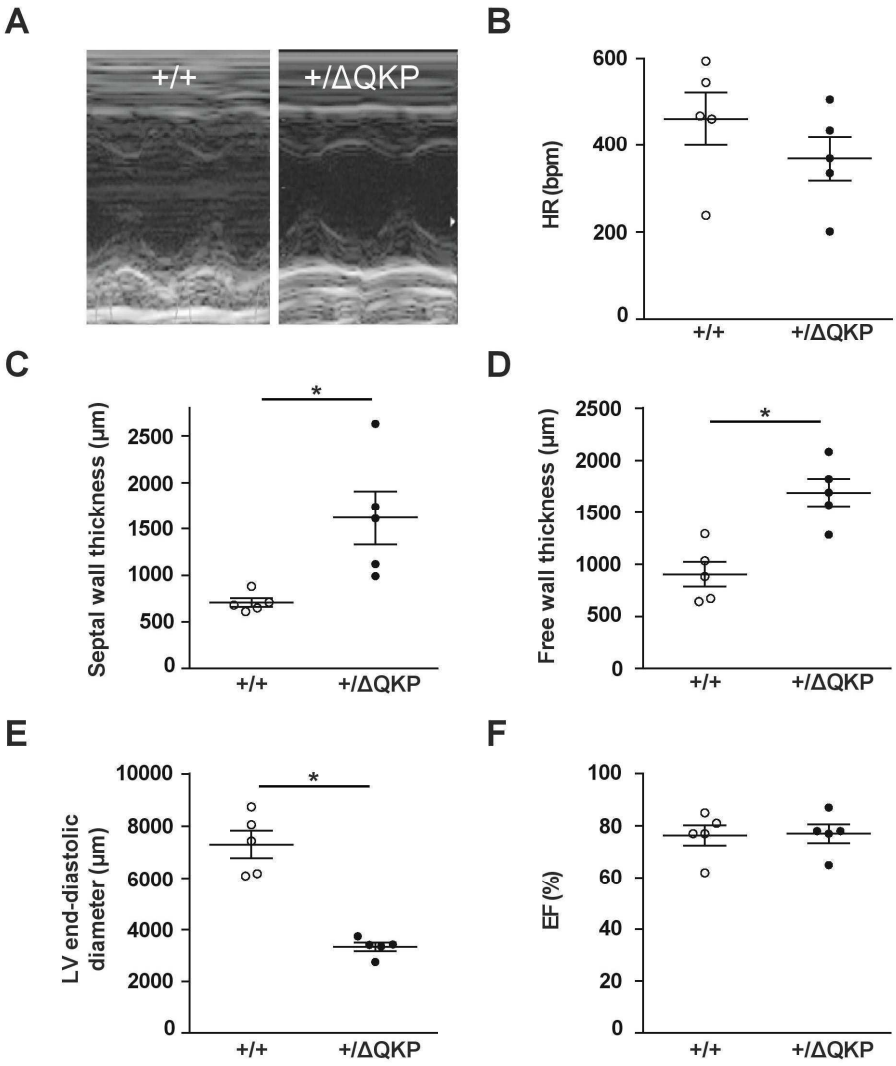


**Supplemental figure 5: signs of left ventricular hypertrophy in *Scn5a*$^{+/\Delta QKP}$ mice.** (**A**) Representative 2-D echocardiography images of the left ventricle of 4-week old *Scn5a*$^{+/+}$ and *Scn5a*$^{+/\Delta QKP}$ mice in sinus rhythm. Heart rate (HR) (**B**), structural remodeling (**C**, **D** and **E**) and systolic function (**F**) were assessed (n = 5 in each group). * P< 0.05 (Mann-Whitney test).

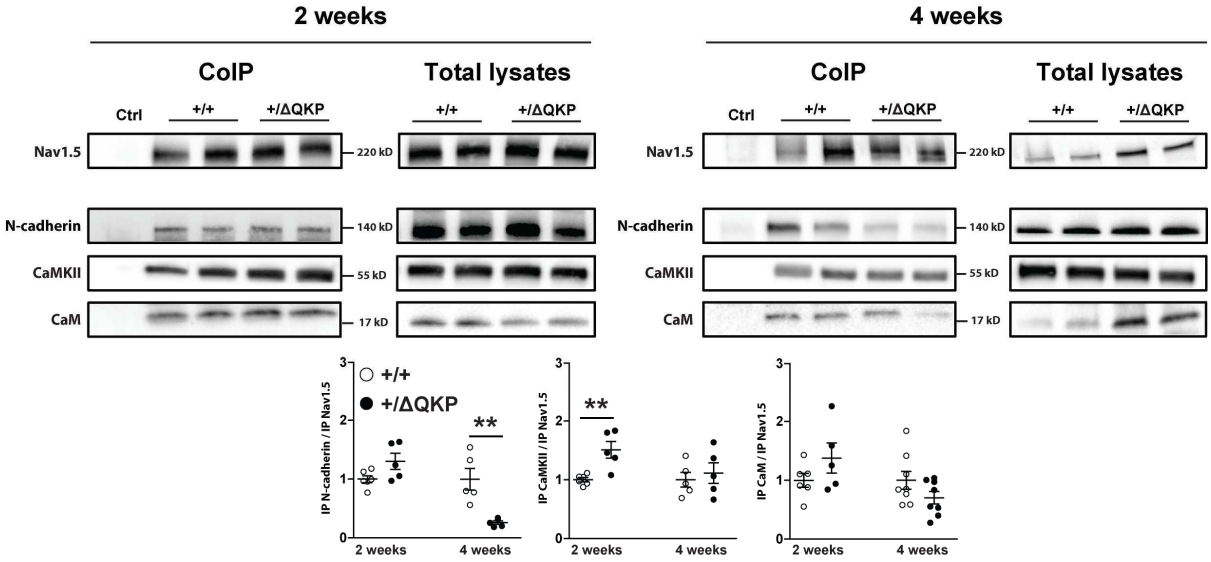


**Supplemental figure 6: Changes in interactions of Nav1.5 and various components of the Nav1.5 macromolecular complex in *Scn5a*$^{+/\Delta QKP}$ mice.** Representative Nav1.5, N-cadherin, $Ca^{2+}$-calmodulin-dependent kinase II (CaMKII) and calmodulin (CaM) western blots of immunoprecipitated proteins and total lysates from left ventricles of 2-week (left) and 4-week (right) old *Scn5a*$^{+/+}$ and *Scn5a*$^{+/\Delta QKP}$ mice (n = 5–8) probed with anti-Nav1.5 rabbit monoclonal antibody. Protein abundance is expressed as the ratio of precipitated protein signal to precipitated Nav1.5, normalized to the mean ratio in the *Scn5a*$^{+/+}$ condition. ** $P < 0.01$ (Mann-Whitney test).

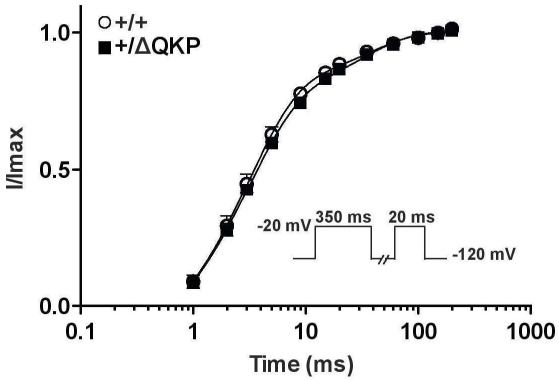


**Supplemental figure 7: recovery from inactivation of cardiac $Na^+$ current.** Fractional recovery from inactivation in *Scn5a*$^{+/+}$, and *Scn5a*$^{+/\Delta QKP}$ cardiomyocytes (n = 11 from 6 mice and 5 from 3 mice, respectively) measured using a twin protocol (inset, 0.2 Hz). The data are the mean fractional current measured during the 2$^{nd}$ depolarization pulse following a repolarization to -120 mV for various durations after the 1$^{st}$ depolarization pulse.

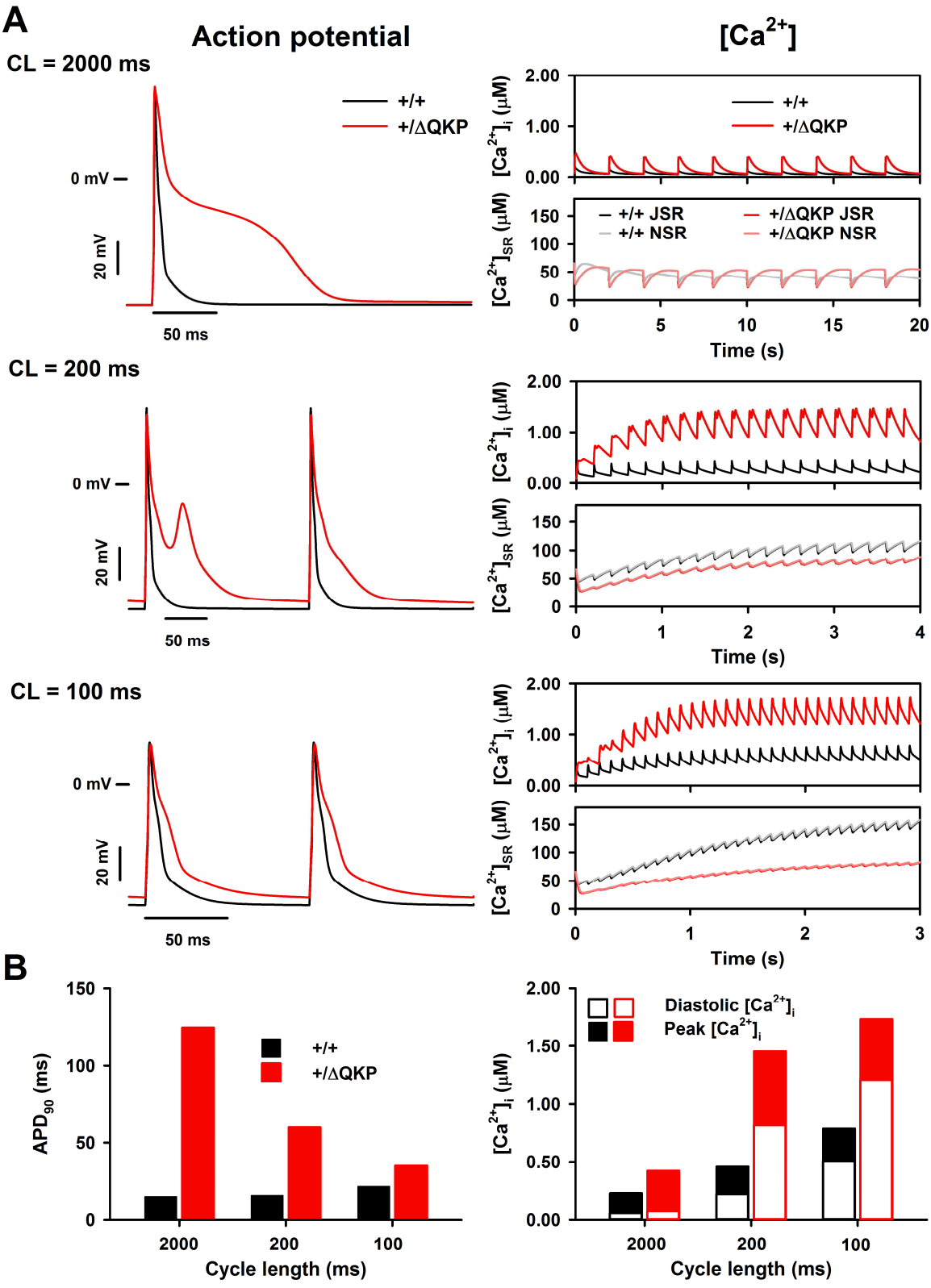
A
Action potential
[Ca2+]
CL = 2000 ms
+/+
+/ΔQKP
0 mV
20 mV
50 ms
[Ca2+]i (μM)
[Ca2+]SR (μM)
+/+ JSR
+/+ NSR
+/ΔQKP JSR
+/ΔQKP NSR
Time (s)
CL = 200 ms
CL = 100 ms
B
APD90 (ms)
Cycle length (ms)
Diastolic [Ca2+]i
Peak [Ca2+]i

**Supplemental figure 8: i*n silico* model of *Scn5a*$^{+/\Delta QKP}$ predicts an increase of both $APD_{90}$ and $[Ca^{2+}]_i$ compared to wildtype condition at cycle lengths of 2000, 200 and 100 ms. A**. *Left panels*: simulated action potentials of *Scn5a*$^{+/+}$ and *Scn5a*$^{+/\Delta QKP}$ ventricular cardiomyocytes at steady-state at cycle lengths of 2000 ms (top), 200 ms (middle) or 100 ms (bottom). *Right panels*: respective cytoplasmic ($[Ca^{2+}]_i$; top) and junctional, (JSR), and non-junctional (NSR) sarcoplasmic reticulum $[Ca^{2+}]$, ($[Ca^{2+}]_{SR}$; bottom) until steady-state. Initial values of the models correspond to the CellML default values. **B**. Simulated values of $APD_{90}$ (left panel) and of diastolic and peak $[Ca^{2+}]_i$ (right panel) in *Scn5a*$^{+/+}$ and *Scn5a*$^{+/\Delta QKP}$ cardiomyocytes at cycle lengths of 2000, 200 and 100 ms at steady-state.

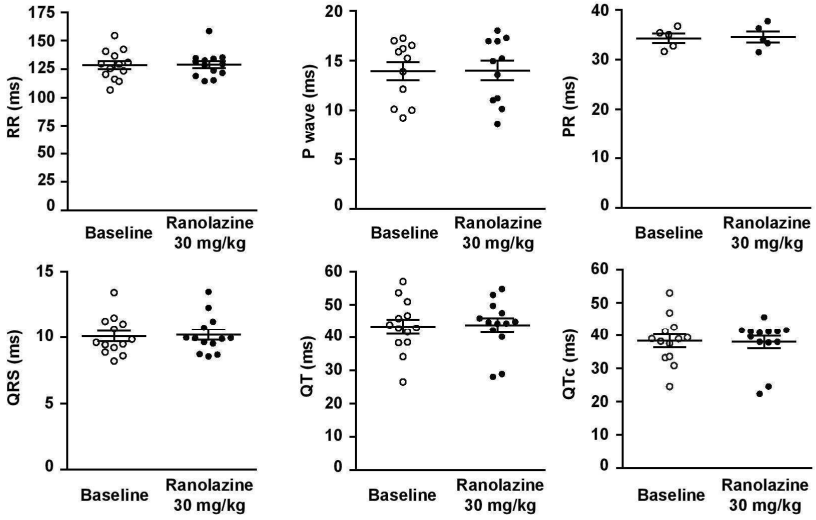


**Supplemental figure 9: ranolazine has no cardiac effect in *Scn5a*$^{+/+}$ mice.** ECG parameters in *Scn5a*$^{+/+}$ mice at baseline and 10 min after ranolazine injection (IP, 30 mg/kg, n = 5-13).

## References


1 Royer A, van Veen TAB, Le Bouter S, Marionneau C, Griol-Charhbili V, Leoni A-L, Steenman M, van Rijen HVM, Demolombe S, Goddard CA, Richer C, Escoubet B, Jarry-Guichard T, Colledge WH, Gros D, de Bakker JMT, Grace AA, Escande D, Charpentier F. Mouse model of SCN5A-linked hereditary Lenègre's disease: age-related conduction slowing and myocardial fibrosis. *Circulation*. 2005;**111**:1738–1746.

2 Derangeon M, Montnach J, Cerpa CO, Jagu B, Patin J, Toumaniantz G, Girardeau A, Huang CLH, Colledge WH, Grace AA, Baró I, Charpentier F. Transforming growth factor β receptor inhibition prevents ventricular fibrosis in a mouse model of progressive cardiac conduction disease. *Cardiovasc Res.* 2017;113:464-474.

3 Rajamani S, El-Bizri N, Shryock JC, Makielski JC, Belardinelli L. Use-dependent block of cardiac late $Na^+$ current by ranolazine. *Heart Rhythm*. 2009;**6**:1625–1631.

4 Fredj S, Sampson KJ, Liu H, Kass RS. Molecular basis of ranolazine block of LQT-3 mutant sodium channels: evidence for site of action. Br J Pharmacol. 2009;148:16–24.

5 Gómez AM, Cheng H, Lederer WJ, Bers DM. $Ca^{2+}$ diffusion and sarcoplasmic reticulum transport both contribute to $[Ca^{2+}]i$ decline during $Ca^{2+}$ sparks in rat ventricular myocytes. *J Physiol (Lond)*. 1996;**496 (Pt 2)**:575–581.

6 Cheng H, Song LS, Shirokova N, Gonzalez A, Lakatta EG, Ríos E, Stern MD. Amplitude distribution of calcium sparks in confocal images: theory and studies with an automatic detection method. *Biophys J*. 1999;**76**:606–617.

7 Williams S, Pourrier M, McAfee D, Lin S, Fedida D. Ranolazine improves diastolic function in spontaneously hypertensive rats. *Am J Physiol Heart Circ Physiol*. 2014;**306**:H867–H881.

8 Wagner E, Brandenburg S, Kohl T, Lehnart SE. Analysis of tubular membrane networks in cardiac myocytes from atria and ventricles. *J Vis Exp*. 2014;(**92**):e51823.

9 Pandit SV, Clark RB, Giles WR, Demir SS. 2001 - Mouse ventricular myocyte model, https://models.cellml.org/exposure/ea62c9c8a502afe364350d353ebf4dd5 12th January 2017. CellML author: Catherine Lloyd.

10 Wang DW, Yazawa K, George AL Jr, Bennett PB. Characterization of human cardiac $Na^+$ channel mutations in the congenital long QT syndrome. *Proc Natl Acad Sci U S A*. 1996;**93**:13200-13205.

11 Pandit SV, Clark RB, Giles WR, Demir SS. A mathematical model of action potential heterogeneity in adult rat left ventricular myocytes. *Biophys J.* 2001;**81**:3029-3051.